consulting
scientists and
engineers

MEMORANDUM

MFG PROJECT: 180734

TO: Dr. A. K. Ibrahim, U.S. Nuclear Regulatory Commission

FROM: Roslyn Stern, Clint Strachan

DATE: December 21, 2004

SUBJECT: **Sequoyah Fuels Corporation Site, Seismicity Issues**

COPY: Craig Harlin, Sequoyah Fuels Corporation

This memorandum has been prepared to provide additional information on the seismicity issues discussed in our telephone conversation on November 3, 2004. During this telephone conversation, five issues were discussed, as a follow-up to the June 22, 2004 response to the NRC Request for Additional Information (RAI) (SFC, 2004) and the subsequent memorandum with additional information dated September 7, 2004. These issues are outlined below.

1. Is Fault 70 in Table 6 of September 7, 2004 memo considered capable?

In Table 6, all faults have been determined not capable per the Black Fox report. This statement was inadvertently left off of fault 70.

2. Verify the definition of magnitude used to calculate horizontal accelerations in Table A.1 and Table 6 of September 7, 2004 memo

The relationship developed by Slemmons (1982) correlates fault length to surface wave magnitude (M_s). The attenuation relationships developed to correlate magnitude and distance to peak horizontal accelerations are based on various definitions of magnitude. Campbell (1981) uses M_s for magnitudes greater than 6.0 and local magnitude (M_l) for magnitudes less than 6.0. Atkinson and Boore (1995) use moment magnitudes (M_w) in their relationships, as does Campbell in his 2003 paper. In Tables A.1 and 6 presented in the September 7, 2004 memo, the magnitudes calculated based on fault length were incorrectly reduced using a conversion from Nuttli magnitude (M_n) to moment magnitude for magnitudes less than or equal to 6.0. Studies (Wells and Coopersmith, 1994, Kanamori, 1983) have shown that in the range of 5.0 to 7.5, M_s and M_w are approximately equal. Therefore, Table 6 is represented below corrected for attenuation calculated using M_s. The corrected version of Table A.1 is shown in Attachment 1.

MFG, Inc.
3801 Automation Way, Suite 100
Fort Collins, CO 80525
Phone: 970-223-9600 *Fax: 970-223-7171*

3. Explain why fault 83, with MCE 6.1 and a distance of 14 km from site has a peak horizontal acceleration of 0.45 g while fault 70, with MCE 6.0 and a distance of 14 km from site has a peak horizontal acceleration of only 0.28 g.

As explained in comment 2, MCE equal or below 6.0 were mistakenly reduced using an M_n to M_w correlation. Therefore, for the attenuation relationship, the magnitude for fault 70 was incorrectly reduced to 5.5. This correction has been made in Tables 6 and A.1 in this letter. This correction has little impact on the final seismic assessment for the Sequoyah Fuels site since all faults in the region have been determined to be inactive faults.

4. Assuming the random earthquake events can be limited to a magnitude of 6.2, what is the calculated peak horizontal acceleration if this event is applied 15 km from the site?

Using Atkinson and Boore (1995) attenuation equations, the computed horizontal acceleration is 0.46 g. Using the original magnitude-frequency curve as shown in Figure 1, the annual probability of having an event of this size occur within this distance is approximately 1/75,000. If the magnitude-frequency curve from LaForge (1997) is used (discussed further in comment 5), the annual probability of occurrence is 1/900,000.

5. Dr. Ibrahim commented that he didn't feel comfortable with the explanation of using concentric circles about the site as source zones for the random earthquake analysis, and didn't agree with the larger circles (i.e. source zones) having larger 10,000-year earthquake events associated with them as presented in Tables 1 and 3 of the September 7, 2004 letter. Provide additional documentation to support technique and results for the random earthquake analysis.

In 1997, Roland LaForge issued a report on the seismic hazards associated with seven dams owned by the U.S. Bureau of Reclamation (USBR) in Oklahoma (LaForge, 1997). One of these dams is the McGee Creek dam, an earthfilled dam with a height of 161 feet. The dam is located approximately 90 miles southwest of the site in Atoka County, in the Ouachita Uplift geologic province. In 2004, LaForge issued a draft update to his seismic hazard assessment (LaForge, 2004). The following is a summary of the approach used in these reports by LaForge to evaluate the peak horizontal accelerations associated with the McGee Creek dam. In addition, because both the McGee Creek and Sequoyah Fuels sites are within LaForge's study zone, a comparison between seismicity rates and horizontal acceleration results are also made. A copy of the 1997 paper and the 2004 update is included in Attachment 2.

Area of study

In LaForge's study, Oklahoma was divided into three areas based on historical seismicity patterns. Clusters of higher activity were observed in the mid to south-central portion of the state. The area east of these clusters is defined by LaForge as Zone 3, and includes the McGee Creek dam and the Sequoyah Fuels site. The considered seismic hazards to the McGee Creek dam include the Meers fault and randomly occurring events within Zone 3. However, the Meers fault is 230 km from the McGee Creek site and 300 km from the Sequoyah Fuels site. Probabilistically, impacts on either site from the Meers fault are considered insignificant.

Probabilistic seismic hazard approach

In accordance with current USBR practice, LaForge used a rigorous probabilistic approach in estimating the seismic hazard where the ground motion associated with a desired probability of exceedance is estimated. In this approach, the ground motion at a given probability of exceedance is not associated with a specific seismic event. In calculating seismic hazards, LaForge accounted for the variability in all the

parameters that are part of estimating site accelerations. Specifically, the probability of ground motion exceedance was calculated by:

$$P(v \geq V) = \sum_{S} \iint P(v \geq V) \,|(m,r))P(m)P(r)dmdr$$

Where $P(v \geq V)$ is the probability that ground motion v exceeds some value V, from all possible sources S.

$P(v \geq V \,|(m,r)$ is the probability that ground motion v exceeds value V given a magnitude and distance.

$P(m)$ is the probability of an event occurring with a given magnitude anywhere within the seismic province under consideration.

$P(r)$ is the probability that an event occurs at a given distance r from the site.

Attenuation Relationships

$P(v \geq V \,|(m,r)$ represents the attenuation relation between magnitude and distance and the accelerations at a site. This is modeled by the attenuation relations chosen. Ground motion attenuation relations for the McGee Creek dam were modeled using EPRI (1993) and Atkinson and Boore (1995). A weighted average 0.67 was assigned to the EPRI model, and 0.33 to the Atkinson and Boore model to reflect LaForge's confidence in the peak horizontal acceleration results. Uncertainties in the attenuation relationships are represented by the lognormal probability density function and are treated in the model by discretizing the distribution into equal-probability values.

Recurrence Calculations

$P(m)$ represents the seismicity rate for the entire source zone. It is modeled by the recurrence curve developed for the site, of the form $Log(N) = a - b(M)$ where N is the number of earthquakes of magnitude M. The data was declustered and corrected for completeness intervals. Declustering is a process of eliminating foreshocks and aftershocks of a main event so that all events can be assumed to be independent events as is necessary for a Poissonian distribution. A declustering algorithm was used to eliminate spatially and temporal dependent events.

In addition, LaForge estimated the completeness interval of the historical seismic data to account for the ability to detect smaller magnitude earthquakes in recent history. Records of events with a body-wave magnitude (mb) 4.0 through 5.0 are considered complete since 1930, 3.0 through 4.0 since 1973, and 2.0 through 3.0 since 1977. LaForge discusses normalizing the recurrence parameters to events per year per square kilometer. In addition to the mean parameters, parameters are developed to provide upper and lower bounds of the 95% confidence interval.

The maximum magnitude associated with a random event in Zone 3 was limited to mb of 6.0. This assumes that events of higher magnitudes are typically associated with known fault features and are not random event.

Location of Event

P(r) is the probability that an event occurring within the source zone will occur at a given distance r from the site. For an area of uniform seismic activity, this probability is equal to A_r/A_p where A_r is the area associated with a given distance r and A_p is the area of the seismic province. In order to analyze the probabilistic seismic hazard for the McGee Creek dam, a gridded point-source model was used to distribute seismicity uniformly across the zone. A grid spacing of 5 km was used. Because the source zone is divided into 5 km grid spacing, the number of r distances an event can occur at is finite and is

equal to 25 km^2. Likewise, the probability of the occurrence of an event of a given magnitude at a given location can be calculated as P(m) * P(r).

Computation
Uncertainties in attenuation and seismicity rate were accounted for by discretizing the lognormal probability density function of each parameter into 50 equal-probability values, resulting in 2500 models. These 2500 models were integrated into the acceleration exceedance model.

Results
As shown in the attached figure (Figure 2 , draft report dated 10/5/04, shown in Attachment 2), the peak horizontal acceleration associated with the mean percentile, 1E-4 annual probability of exceedance is 0.16g.

Discussion of results and methodology as compared to those used by MFG
Several main differences between the LaForge analysis and the analysis by MFG should be noted.

- The ground motion recurrence relationships developed by LaForge are the result of the integration of probabilities of occurrence for all possible events, and thus, are not associated with any specific seismic event. The advantage of this method is that it allows an estimation of the 10,000-year ground motion. The more deterministic approach used by MFG calculates ground motion by applying a 10,000-year event at an assumed location and by using a mean attenuation relationship.
- LaForge used a more rigorous technique to develop the recurrence interval of seismic events. This included correcting for completeness record and declustering dependent events. Figure 1 shows the original magnitude frequency curve developed by MFG, a revised MFG curve corrected for completeness record, and the curve developed by LaForge for Zone 3. It should be noted that LaForge's curve has been modified as presented in LaForge (1997) to represent cumulative frequency, rather than incremental, and adjusted for an equivalent area of the Ozark Uplift. The LaForge and MFG revised curves are similar, especially when considering that the source zones are slightly different (eastern Oklahoma of 65,000 km^2 versus the Ozark Uplift of 322,000 km^2).
- The probabilistic seismic hazard analysis approach used by LaForge uses probability distributions as input parameters and produces ground motion probability distributions as output. MFG used mean values for attenuation, and a single magnitude-frequency relationship; LaForge's analysis incorporates the variability of these parameters.

It should be noted that in both LaForge's and MFG's analyses, the magnitude-frequency relationship for the province P(m) is adjusted using the probability of occurrence at a specific location P(r) when estimating the probability of occurrence of a given event at a given location. In both studies this adjustment is made by taking the product of P(m) * P(r) where P(m) applies to the whole province and P(r) is calculated by A_r/A_p (as defined previously). In LaForge's analysis, the probabilistic model generates seismic events emanating from 25 km^2 grids. Had LaForge chosen a larger grid spacing, the model would have generated a higher probability for any given magnitude event, but the event could occur at fewer grid points. The closest grid points would be farther away from the site than the grid points under a tighter spacing. In the MFG model, the 10,000-year event is calculated from a circular area concentric about the site. Once an event is calculated for a circular or a grid area, the question becomes where to place the event in order to apply the attenuation equation (in both analyses). LaForge chose to apply the event at the centroid of the square grid which represents the mean distance of the grid area from the site. Since MFG evaluated concentric circles about the site, the event was placed at the mean radius from the site. As a comparison, had MFG used the same recurrence interval as LaForge, the 10,000-year event for a 25 km^2 circle centered at the site, (3.1 magnitude event applied 1.98 km from the

site) and the mean attenuation values as developed by Atkinson and Boore (1995), the computed peak ground acceleration is 0.14g, as compared to 0.16g by LaForge.

We trust that this memorandum addresses remaining questions regarding the seismicity analysis for the Sequoyah Fuels site. MFG feels that the approach used in the analysis, while not as rigorous as that described by LaForge, does produce similar or more conservative ground motions at the 10,000-year recurrence level. The ability of the disposal cell to withstand a peak horizontal acceleration of 0.27 g is considered to be adequately conservative.

Table 6 Maximum Credible Earthquake and Site Ground Vibratory Motion for Critical Faults with Potential Horizontal Accelerations Greater than 0.27 g.

Fault ID	Fault Length (km)	Dist. from Site (km)	MCE (Slemmons 1982)	Hor. Accel. at Site Campbell 2003 (g)	Black Fox (BF) Fault ID	BF Fault Name	Tectonic Province (1)	Comments
103	42.1	1	7.0	1.403	91	Lyons	OU	BF fault 91 extends farther north than fault 103 of this report. Marble City fault, not capable per NRC Dec. 3, 1998 letter to James Shepherd (SFC). Lyons fault not capable per BF report.
99	4.4	8	5.7	0.641	78	Webbers Cove	AB	South Fault of Warner Uplift. Segments 35, 101, 12, 99, and 33 in this report considered collectively as Webbers Cove Fault in BF report. Fault not capable per BF report and NRC Dec. 3, 1998 letter to James Shepherd (SFC).
33	3.1	9	5.5	0.503	78	Webbers Cove	AB	Segments 35, 101, 12, 99, and 33 in this report considered collectively as Webbers Cove Fault in BF report. Fault not capable per BF report.
95	15.7	16	6.4	0.464	77	Greenleaf Lake	OU	Northern part forms horst with southern part of South Qualls fault (83 of BF report). Fault not capable per BF report.
83	9.0	14	6.1	0.450	85		AB	Segments 70 and 83 of this report considered collectively as fault 85 in BF report. Fault not capable per BF report.
50	21.1	19	6.6	0.416	50		AB	Fault not capable per BF report.
70	7.2	14	6.0	0.402	85			Segments 70 and 83 of this report considered collectively as fault 85 in BF report. Fault not capable per BF report.
39	5.3	14	5.8	0.355	79		CP	Fault not capable per BF report.
18	4.6	14	5.7	0.352	94	Akins	OU	Segments 18, 66, 56, and 65 considered collectively as fault 94 in BF report. Fault not capable per BF report.
68	3.0	12	5.5	0.348			OU	Fault not addressed specifically in BF report, but covered generally with Ozark Uplift faults. Not capable per BF report.
81	14.4	20	6.4	0.346			AB	Fault not addressed specifically in BF report, but covered generally with Arkoma Basin faults. Not capable per BF report.
49	11.0	19	6.2	0.338	88	Black Gum	OU	Fault not capable per BF report.
20	5.7	15	5.8	0.336	90		OU	Segments 20, 57, and 80 considered collectively as fault 90 in BF report. Fault not capable per BF report.
22	18.6	23	6.5	0.323	82	Qualls-Welling	OU	Segments 22 and 119 in this report considered collectively as fault 82 in BF report. Fault not capable per BF report.
35	3.4	13	5.5	0.322	78	Webbers Cove	AB	Segments 35, 101, 12, 99, and 33 in this report considered collectively as Webbers Cove Fault in BF report. Fault not capable per BF report.
85	9.7	19	6.2	0.321	83	South Qualls	OU	Fault not capable per BF report.
79	29.5	27	6.8	0.300	93	Greasy Creek	OU	Intersects the north end of the Atkins fault (94 of BF report). Fault not capable per BF report.
57	9.5	20	6.1	0.296	90		OU	Segments 20, 57, and 80 considered collectively as fault 90 in BF report. Fault not capable per BF report.
69	3.2	14	5.5	0.286			OU	Fault not addressed specifically in BF report, but covered generally with Ozark Uplift faults. Not capable per BF report.
78	8.5	20	6.1	0.278	27	Keefeton	CP	Segments 31 and 78 considered collectively as fault 27 in BF report. Fault not capable per BF report.
37	15.2	25	6.4	0.254	95		OU	Fault 95 in BF report shown extending north to Akins fault. Fault not capable per BF report.
102	32.9	32	6.9	0.250	12		CP	Fault not capable per BF report.
53	28.3	31	6.8	0.246	78A	S. Muskogee	OU	Fault not capable per BF report.

(1) OU = Ozark Uplift; AB = Arkoma Basin; CP = Cherokee Platform

References Cited in This Memorandum

Atkinson, G. M., and Boore, D. M., 1995. Ground-Motion Relations for Eastern North America, Bulletin of the Seismological Society of America, Vol. 85, No. 1, pp. 17-30, February.

Campbell, K.W., 1981. Near-Source Attenuation of Peak Horizontal Acceleration, *Bulletin of the Seismological Society of America*, Vol. 71, No. 6, pp. 2039-2070, December.

Campbell, K.W., 2003. Prediction of Strong Ground Motion using the Hybrid Empirical Method and Its Use in the Development of Ground-Motion (Attenuation) Relations in Eastern North America, *Bulletin of the Seismological Society of America*, Vol. 93, No. 3, pp. 1012-1033, June.

Kanamori, H., 1983. Magnitude scale and quantification of earthquakes, Tectonophysics vol. 93, 185-199.

LaForge, R, 1997. Seismic Hazard and Ground Motion Analyses for Altus, Arbuckle, Fort Cobb, Foss, McGee Creek, Mountain Park, and Norman Dams, Oklahoma, Seismotectonic Report 97-1, U.S. Bureau of Reclamation, July.

LaForge, Roland (2001). mrs Programs for Site-Specific Probabilistic Seismic Hazard Analysis for Zones of Random Seismicity, Technical Memorandum No. D 8330-2001-13, Bureau of Reclamation, June.

LaForge, R, 2004. Draft Comprehensive Facility Review, McGee Creek Dam Seismic Hazard, unpublished.

MFG, Inc. (MFG), 2003. "Sequoyah Fuels Corporation Facility Seismicity Evaluation." Prepared for Sequoyah Fuels Corporation. July.

Sequoyah Fuels Corporation (SFC), 2004. "Response to: Request for Additional Information Reclamation Plan." Prepared for U.S. Nuclear Regulatory Commission. June 22.

Shannon and Wilson, Inc. 1975. "Geotechnical Investigations, Black Fox Station, Rogers County, Oklahoma." To Black and Veatch for Public Service Company of Oklahoma. April.

U.S. Nuclear Regulatory Commission (NRC), 1997. "Nuclear regulatory Commission Staff's Evaluations of Sequoyah Fuel Corporation's Response to NRC's Questions Related to Seismic Conditions Near the Sequoyah Facility." Letter to John H. Ellis, SFC, from John W. N. Hickey, NRC, December 15, 1997.

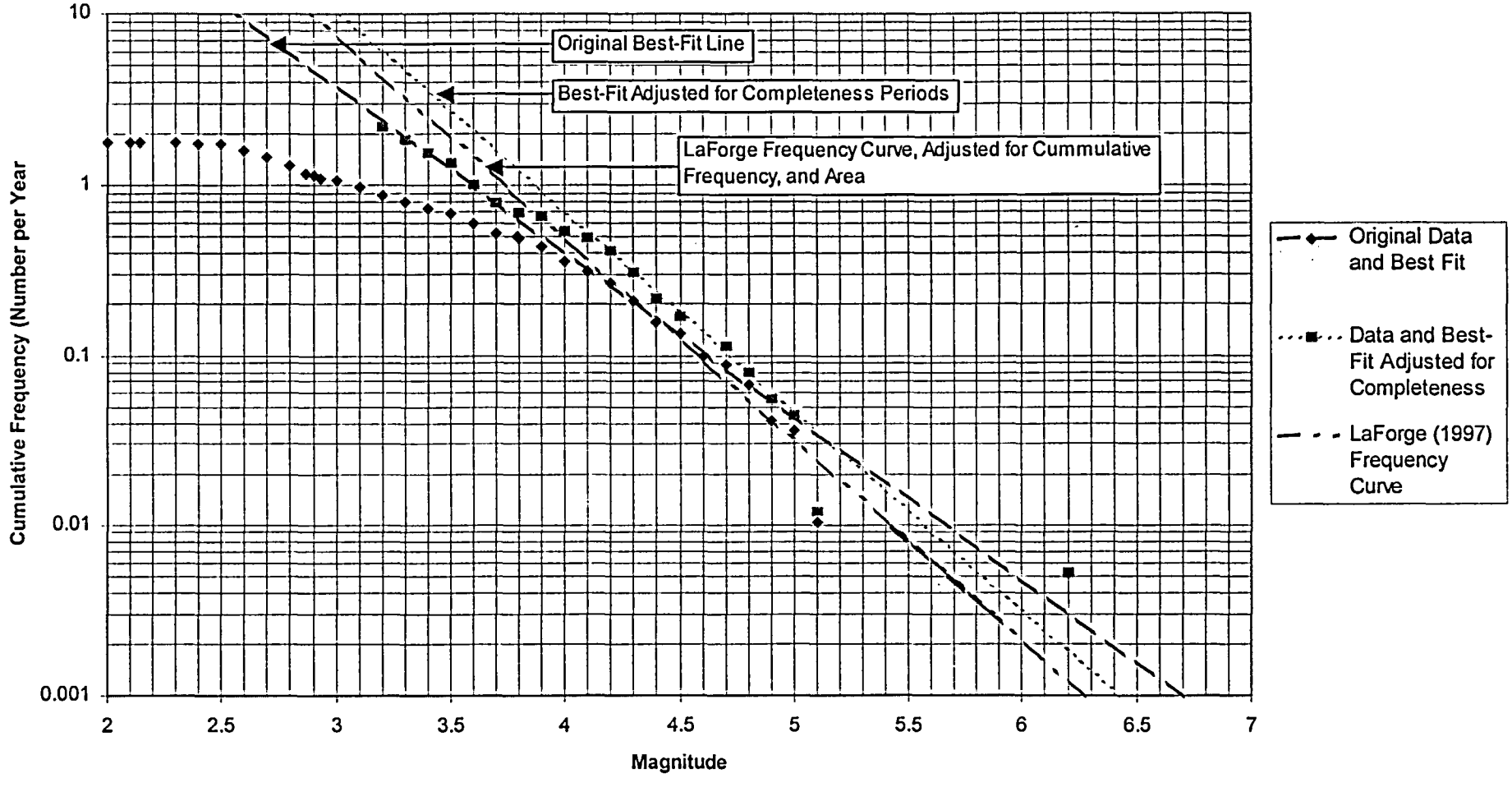

MFG, Inc. *consulting scientists and engineers*	FIGURE 1 Magnitude-Frequency Curve Ozark Uplift

Date:	December 2004
Project:	P:\100734\Seismicity
File:	Fig 1 Dec04 memo

Attachment 1

Table A.1 Maximum Credible Earthquake and Site Ground Vibratory Motion for Critical Faults

Table A.1. Maximum Credible Earthquake and Site Ground Vibratory Motion for Critical Faults

Fault ID [1]	Fault Length (km)	Distance from Site (km)	MCE (Slemmons, 1982, normal faults)	MCE (Slemmons, 1982, reverse faults)	Horizontal Acceleration at Site (Campbell, 1981) (g)	Horizontal Acceleration at Site (Atkinson and Boore, 1995) (g)	Horizontal Acceleration at Site (Campbell, 2003) (g)	Comments
Faults Located Within 20 miles of Site								
103	42.1	1	7.0		0.661	22.127	1.403	Marble City fault, not capable
79	29.5	27	6.8		0.124	0.340	0.300	Not capable, per BF report
53	28.3	31	6.8		0.108	0.292	0.246	Not capable, per BF report
50	21.1	19	6.6		0.145	0.446	0.416	Not capable, per BF report
22	18.6	23	6.5		0.120	0.363	0.323	Not capable, per BF report
95	15.7	16	6.4		0.150	0.492	0.464	Not capable, per BF report
37	15.2	25	6.4		0.100	0.300	0.254	Not capable, per BF report
82	15.2	28	6.4		0.092	0.273	0.224	Not capable, per BF report
81	14.4	20	6.4		0.121	0.383	0.346	Not capable, per BF report
65	11.9	30	6.3		0.076	0.226	0.175	Not capable, per BF report
49	11.0	19	6.2		0.115	0.373	0.338	Not capable, per BF report
93	10.0	25	6.2		0.086	0.267	0.221	Not capable, per BF report
85	9.7	19	6.2		0.109	0.356	0.321	Not capable, per BF report
57	9.5	20	6.1		0.103	0.333	0.296	Not capable, per BF report
52	9.3	31	6.1		0.068	0.205	0.154	Not capable, per BF report
83	9.0	14	6.1		0.136	0.473	0.450	Not capable, per BF report
58	8.8	23	6.1		0.085	0.269	0.225	Not capable, per BF report
77	8.5	26	6.1		0.076	0.238	0.191	Not capable, per BF report
78	8.5	20	6.1		0.097	0.316	0.278	Not capable, per BF report
56	8.2	22	6.1		0.087	0.277	0.235	Not capable, per BF report
31	7.9	29	6.0		0.066	0.203	0.154	Not capable, per BF report
43	7.6	21	6.0		0.088	0.283	0.243	Not capable, per BF report
76	7.5	30	6.0		0.063	0.193	0.145	Not capable, per BF report
70	7.2	14	6.0		0.122	0.423	0.402	Not capable, per BF report
74	6.6	32	5.9		0.056	0.172	0.125	Not capable, per BF report
6	6.2	29	5.9		0.059	0.182	0.136	Not capable, per BF report
24	6.2	25	5.9		0.069	0.218	0.174	Not capable, per BF report
45	6.0	27	5.9		0.064	0.200	0.155	Not capable, per BF report
72	5.8	23	5.9		0.071	0.227	0.185	Not capable, per BF report
20	5.7	15	5.8		0.105	0.358	0.336	Not capable, per BF report
80	5.5	29	5.8		0.056	0.176	0.131	Not capable, per BF report
75	5.4	30	5.8		0.054	0.168	0.123	Not capable, per BF report
39	5.3	14	5.8		0.108	0.372	0.355	Not capable, per BF report
63	5.2	26	5.8		0.060	0.190	0.147	Not capable, per BF report
48	5.1	28	5.8		0.056	0.175	0.131	Not capable, per BF report
97	4.9	27	5.8		0.058	0.184	0.141	Not capable, per BF report
62	4.8	28	5.7		0.055	0.172	0.128	Not capable, per BF report
23	4.6	29	5.7		0.052	0.164	0.121	Not capable, per BF report

Table A.1. Maximum Credible Earthquake and Site Ground Vibratory Motion for Critical Faults (cont)

Fault ID	Fault Length (km)	Distance from Site (km)	MCE (Slemmons, 1982, normal faults)	MCE (Slemmons, 1982, reverse faults)	Horizontal Acceleration at Site (Campbell, 1981) (g)	Horizontal Acceleration at Site (Atkinson and Boore, 1995) (g)	Horizontal Acceleration at Site (Campbell, 2003) (g)	Comments
Faults Located Within 20 miles of Site								
18	4.6	14	5.7		0.105	0.366	0.352	Not capable, per BF report
59	4.6	29	5.7		0.052	0.163	0.120	Not capable, per BF report
99	4.4	8	5.7		0.168	0.659	0.641	South Fault of Warner Uplift, not capable
41	4.2	29	5.7		0.050	0.159	0.117	Not capable, per BF report
27	4.0	20	5.6		0.070	0.229	0.197	Not capable, per BF report
46	4.0	31	5.6		0.045	0.140	0.098	Not capable, per BF report
73	3.9	30	5.6		0.047	0.147	0.106	Not capable, per BF report
47	3.8	32	5.6		0.043	0.134	0.093	Not capable, per BF report
66	3.7	18	5.6		0.075	0.249	0.221	Not capable, per BF report
71	3.5	24	5.6		0.056	0.179	0.142	Not capable, per BF report
35	3.4	13	5.5		0.095	0.330	0.322	Not capable, per BF report
44	3.4	22	5.5		0.058	0.187	0.153	Not capable, per BF report
42	3.2	20	5.5		0.062	0.203	0.172	Not capable, per BF report
51	3.2	27	5.5		0.048	0.152	0.114	Not capable, per BF report
69	3.2	14	5.5		0.087	0.298	0.286	Not capable, per BF report
38	3.1	26	5.5		0.049	0.157	0.120	Not capable, per BF report
26	3.1	23	5.5		0.054	0.175	0.140	Not capable, per BF report
33	3.1	9	5.5		0.132	0.490	0.503	Not capable, per BF report
29	3.1	26	5.5		0.048	0.153	0.117	Not capable, per BF report
68	3.0	12	5.5		0.100	0.348	0.348	Not capable, per BF report
Hypothetical	3.0	8	5.5		0.137	0.514	0.527	
Faults Located Within 50 Miles of Site								
102	32.9	32	6.9		0.112	0.294	0.250	Not capable, per BF report
105	25.9	39	6.7		0.085	0.220	0.169	Not capable, per BF report
104	22.7	47	6.7		0.068	0.174	0.122	Not capable, per BF report
110	18.9	79		6.9	0.049	0.104	0.073	Not capable, per BF report
111	18.1	73		6.9	0.052	0.114	0.074	Not capable, per BF report
Hypothetical	18.1	32		6.9	0.112	0.293	0.250	
200	50.0	61	7.1		0.074	0.157	0.113	Not capable, per BF report
201	29.4	61	6.8		0.059	0.136	0.089	Not capable, per BF report
203	14.1	74	6.4		0.034	0.086	0.049	Not capable, per BF report
204	12.4	76	6.3		0.031	0.079	0.045	Not capable, per BF report
205	10.6	75	6.2		0.029	0.076	0.042	Not capable, per BF report
202	10.5	63	6.2		0.035	0.095	0.053	Not capable, per BF report
209	10.1	58	6.2		0.038	0.103	0.059	Not capable, per BF report
207	8.5	76	6.1		0.026	0.069	0.038	Not capable, per BF report
208	6.7	79	5.9		0.022	0.060	0.033	Not capable, per BF report
206	4.1	69	5.7		0.020	0.057	0.028	Not capable, per BF report

Table A.1. Maximum Credible Earthquake and Site Ground Vibratory Motion for Critical Faults (cont)

Fault ID	Fault Length (km)	Distance from Site (km)	MCE (Slemmons, 1982, normal faults)	MCE (Slemmons, 1982, reverse faults)	Horizontal Acceleration at Site (Campbell, 1981) (g)	Horizontal Acceleration at Site (Atkinson and Boore, 1995) (g)	Horizontal Acceleration at Site (Campbell, 2003) (g)	Comments
Faults Located Within 100 Miles of Site								
106	36.7	100		7.2	0.050	0.089	0.084	Not capable, per BF report
108	36.2	135	6.9		0.029	0.052	0.054	Not capable, per BF report
107	34.9	123	6.9		0.032	0.059	0.058	Not capable, per BF report
113	26.8	94		7.1	0.048	0.091	0.077	Not capable, per BF report
Hypothetical	26.8	80		7.1	0.055	0.110	0.083	
211	10.2	158		6.6	0.019	0.035	0.033	Not capable, per BF report
216	109.7	145		7.8	0.054	0.063	0.096	Not capable, per BF report
212	76.2	118		7.6	0.057	0.081	0.102	Not capable, per BF report
210	88.7	102	7.4		0.059	0.094	0.098	Not capable, per BF report
217	85.1	147		7.6	0.048	0.060	0.085	Not capable, per BF report
215	61.6	119		7.5	0.052	0.077	0.094	Not capable, per BF report
213	51.5	151		7.4	0.038	0.054	0.068	Not capable, per BF report
214	23.3	105		7.0	0.040	0.076	0.068	Not capable, per BF report
Faults Located Within 150 Miles of Site								
109	118.0	202	7.6		0.034	0.037	0.053	Not capable, per BF report
114	35.6	173	6.9		0.022	0.036	0.037	Not capable, per BF report
219	80.5	162		7.6	0.042	0.051	0.073	Not capable, per BF report
221	72.2	232	7.3		0.023	0.026	0.034	Not capable, per BF report
220	39.3	190	7.0		0.021	0.032	0.034	Not capable, per BF report
Humboldt	---	225.26	6.5		0.012	0.019	0.017	Humboldt
Faults Located Within 200 Miles of Site								
Meers Fault	54.0	306	7.2		0.015	0.015	0.019	Meers Fault

(1) Fault ID corresponds to numbers shown on Figures 3.3 through 3.7 of the MFG (2003) Facility Seismicity Evaluation.

Attachment 2

LaForge, Roland (1997). Seismic Hazard and Ground Motion Analysis for Altus, Arbuckle, Fort Cobb, Foss, McGee Creek, Mountain Park, and Norman Dams, Oklahoma. Seismotectonic Report 97-1, Bureau of Reclamation, July.

With updated figure from

LaForge, Roland (2004). Initial Draft of Comprehensive Facility Review, McGee Creek Dam, Seismic Hazard, October 5.

SEISMIC HAZARD AND GROUND MOTION ANALYSIS

FOR

ALTUS, ARBUCKLE, FORT COBB, FOSS, McGEE CREEK, MOUNTAIN PARK, AND NORMAN DAMS

OKLAHOMA

by

Roland C. LaForge

Seismotectonic Report 97-1

Seismotectonics and Geophysics Group
Geotechnical Services
Technical Service Center
Bureau of Reclamation
Denver, Colorado

July, 1997

Bureau of Reclamation
Technical Service Center
Seismotectonics and Geophysics Group

Seismotectonic Report 97-1

Seismic Hazard and Ground Motion Analysis for Altus, Arbuckle, Fort Cobb, Foss, McGee Creek, Mountain Park, and Norman Dam, Oklahoma

Prepared By

Roland LaForge
Geophysicist

7/2/97
Date

Peer Review

Ute Vetter
Geophysicist

6/25/97
Date

Summary

Ground motions for seven U.S. Bureau of Reclamation dams in Oklahoma are developed in this report. The dams are Altus, Arbuckle, Fort Cobb, Foss, McGee Creek, Mountain Park, and Norman. Results consist of peak horizontal acceleration hazard curves, uniform hazard acceleration response spectra at 5% damping, and acceleration and velocity spectrum intensity. All except the hazard curves are for two return periods, 10,000 and 50,000 years.

The seismic hazard to the dams was modeled as three zones of random seismicity and the Meers fault. The zones of random seismicity were defined solely on the basis of historic seismicity patterns, and bear little relation to known geologic structures. Eastern and western zones consist of large areas of relatively low-level, spatially homogeneous activity. A narrow zone in the mid-to-south central part of the state contains three clusters of activity, the northernmost of which is the location of the m_b 5.0 1952 El Reno event. Maximum magnitudes of m_b 6.0 were estimated for the eastern and western zones, and m_b 6.5 for the central zone.

The Meers fault is a unique feature of central and eastern North America, in that two surface faulting events in the past 10,000 years have occurred on it. Before this time, however, no events can be identified in the previous several hundred thousand years. To account for this temporally non-uniform behavior, the fault was assigned a 70% probability of being active for the life of the dams.

A probabilistic seismic hazard analysis was performed for each dam based on earthquake recurrence statistics developed for the three zones and the Meers fault, incorporating uncertainties in both seismicity rates and ground motion attenuation. The attenuation relations of EPRI (1993) and Atkinson and Boore (1995) for rock sites were used. Mean (50th percentile) results for the two return periods are tabulated below.

Summary Ground Motion Results

Dam	PHA (g)		ASI (cm/sec)		VSI (cm)	
	10,000 yrs	50,000 yrs	10,000 yrs	50,000 yrs	10,000 yrs	50,000 yrs
Altus	.15	.29	144	270	19	35
Arbuckle	.28	.55	246	447	31	56
Fort Cobb	.24	.42	240	478	32	68
Foss	.11	.24	117	231	16	32
McGee Creek	.17	.37	136	272	14	28
Mountain Park	.24	.49	238	501	.34	74
Norman	.29	.59	255	479	32	59

Table of Contents

Summary iii
List of Figures v
List of Tables v

1.0 Introduction 1
1.1 Acknowledgements 1
2.0 Earthquake Recurrence 2
2.1 Catalog Preparation 2
2.2 Tectonic Features, the Meers Fault, Seismicity Patterns, and Zonation 2
2.3 Recurrence Calculations 5
2.3.1 Declustering 5
2.3.2 Completeness Periods 9
2.3.3 Recurrence curves 10
3.0 Probabilistic Seismic Hazard Analysis 14
3.1 Methodology and Inputs 14
3.2 Results 16
3.3 Discussion 17
4.0 References 18

Appendices

Appendix A Results for Altus Dams A-1
Appendix B Results for Arbuckle Dam B-1
Appendix C Results for Fort Cobb Dam C-1
Appendix D Results for Foss Dam D-1
Appendix E Results for McGee Creek Dam E-1
Appendix F Results for Mountain Park Dam F-1
Appendix G Results for Norman Dam G-1

List of Figures

Figure 2-1. Central Oklahoma seismicity, 1987 through December 1996, and zonation boundaries. . . . 3
Figure 2-2. Major tectonic features of Oklahoma, from Luza and Lawson (1981) 4
Figure 2-3. Declustered seismicity, magnitude 1 and greater. . . . 7
Figure 2-4a. Latitude vs. Time for earthquakes shown in figure 2-3 7
Figure 2-4b. Longitude vs. Time for earthquakes shown in figure 2-3 8
Figure 2-5. Completeness period estimates for Oklahoma from various sources, and those used in this report. . . . 8
Figure 2-6. Earthquakes used in recurrence calculations 10
Figure 2-7a. Incremental recurrence curve for Zone 1 11
Figure 2-7b. Incremental recurrence curve for Zone 2 11
Figure 2-7c. Incremental recurrence curve for Zone 3 12
Figure 3-1. Logic tree of attenuation relation choices and Meers fault activity 16

List of Tables

Table 2-1: Estimates of Maximum Epicentral Location Precision and Minimum Magnitude used in Declustering Algorithm 6
Table 2-2a: Completeness Periods and Event Counts Used in Recurrence Calculations, Zone 1 9
Table 2-2b: Completeness Periods and Event Counts Used in Recurrence Calculations, Zones 2 and 3 9
Table 2-3a: Oklahoma Zone 1: Observed and Predicted Return Periods, with Upper and Lower Bounds of 95% Confidence Interval 12
Table 2-3b: Oklahoma Zone 2: Observed and Predicted Return Periods, with Upper and Lower Bounds of 95% Confidence Interval 13
Table 2-3c: Oklahoma Zone 3: Observed and Predicted Return Periods, with Upper and Lower Bounds of 95% Confidence Interval 13
Table 2-4: Recurrence Parameters for Random Seismicity Source Areas 13
Table 3-1: Estimates of Maximum Magnitude (m_b) from Available Publications 15

1.0 Introduction

This report presents the results of a seismic hazard and ground motion assessment for seven dams regulated by the U.S. Bureau of Reclamation in the state of Oklahoma. The report presents historical seismicity, recurrence statistics, and probabilistic ground motion analyses.

Seismicity in Oklahoma can be considered low, compared to more active regions of the western United States. However, at least 2 events in the m_b 5 range have occurred in historic times. The spatial pattern appears relatively homogeneous, with the exception of three clusters of activity that are seen in the south-central part of the state. The northernmost of these was the site of the 1952 m_b 5.0 El Reno event. These features do not obviously correlate with known geologic structures.

Aside from randomly occurring moderate-magnitude seismicity, a hazard is presented by the Meers fault. This feature is unique in that it is the only known fault east of the Rocky Mountains that has identified Holocene surface rupture. It is judged capable of producing events of M_W 7, and the dams located close to it are under greater risk of sustaining damaging ground motions than others in the state.

Ground motions were developed using the probabilistic technique, as described by Cornell (1968). Uncertainties in both seismicity rates and ground motion attenuation were incorporated into the results. The results consist of hazard curves for Peak Horizontal Acceleration (PHA), uniform hazard acceleration response spectra (UHS) and acceleration and velocity spectrum intensities (ASI and VSI; as defined in von Thun and others, 1988) for return periods of 10,000 and 50,000 years.

1.1 Acknowledgements

Dr. James Lawson of the Oklahoma Geological Survey Observatory was most helpful in providing information and the benefit of his experience in regards to the seismicity of Oklahoma. Data from the Oklahoma seismic network were invaluable in developing the results of this study. Thanks also to Bert Swan of Geomatrix Consultants and Keith Kelson of William Lettis and Associates, for sharing results of their geologic studies of the Meers fault.

2.0 Earthquake Recurrence

2.1 Catalog Preparation

The primary source of seismicity used in this study was the earthquake catalog of the Oklahoma Geological Survey Observatory (OGSO). Because magnitudes were not computed for many of the smaller events, magnitudes for such events listed in Geomatrix (1990, Appendix A) were added to the data set. The Geomatrix catalog in turn was derived from magnitude 2 and greater events from the OGSO and Decade of North American Geology (DNAG; Engdahl and Rinehart, 1991) compilations.

Three types of magnitude calculation are listed in the OGSO catalog. In converting these to a single value, the precedence order described by Lawson (1985) was used. All three magnitudes are considered essentially equivalent to m_b. The entire catalog for central Oklahoma is plotted in figure 2-1. The time span covered is 1897 through December, 1996.

The OGSO has operated an 11 station short period seismograph network in Oklahoma since 1977. Because all but two of the stations are located east of longitude 98°W, coverage can be considered better in the central and eastern part of the state.

2.2 Tectonic Features, the Meers Fault, Seismicity Patterns, and Zonation

The major geologic and tectonic provinces of Oklahoma (reprinted from Luza and Lawson, 1981) are shown in figure 2-2. The Wichita, Arbuckle, and Ouachita Mountains and associated basins are part of the Ouachita System, active during Pennsylvanian (~225 m.y.) time. The Nemaha Ridge, a buried structure, trends SSW from Nebraska into Oklahoma, and appears to have been active earlier, in the late Precambrian (Luza and Lawson, 1983). Microseismicity appears to be associated with this feature in Kansas (Hildebrand and others, 1988).

The Meers fault is found along the southern margin of the Frontal Wichita fault system (Harlton, 1963). The fault location is shown in figure 2-1, and its structural relationship to the Wichita Uplift in the cross-section in figure 2-2. It has the distinction of being the only fault with known Quaternary displacement in North America east of the Rocky Mountains. It has been investigated by a number of workers (e.g., Ramelli, 1988; Donovan and others, 1983; Crone and Luza, 1990; Geomatrix, 1990; Swan and others, 1993). Field studies reported in Geomatrix (1990) indicate a fault length of 26 - 37 km and moment magnitude (M_W) of 6.75 to 7.25. Swan and others (1993) report two Holocene surface faulting events, one at 1300-1400 years and one at 2100-2900 years before present. Prior to these two events there is no evidence for surface faulting during the preceding several hundred thousand years. Recent seismicity has not been associated with the fault.

For use in the probabilistic analysis, it is necessary to decide upon magnitudes and activity rates for the Meers fault. It is assumed that the fault is capable of producing M_W 7.0 earthquakes, and any possible smaller magnitude events are ignored. To calculate activity rates, a Holocene rate of 2 events per 10,000 years was used, and it was assumed that earthquake occurrence on the fault is a Poisson process. In statistical terms, a "success" is counted as one or more earthquakes in time period *t*.

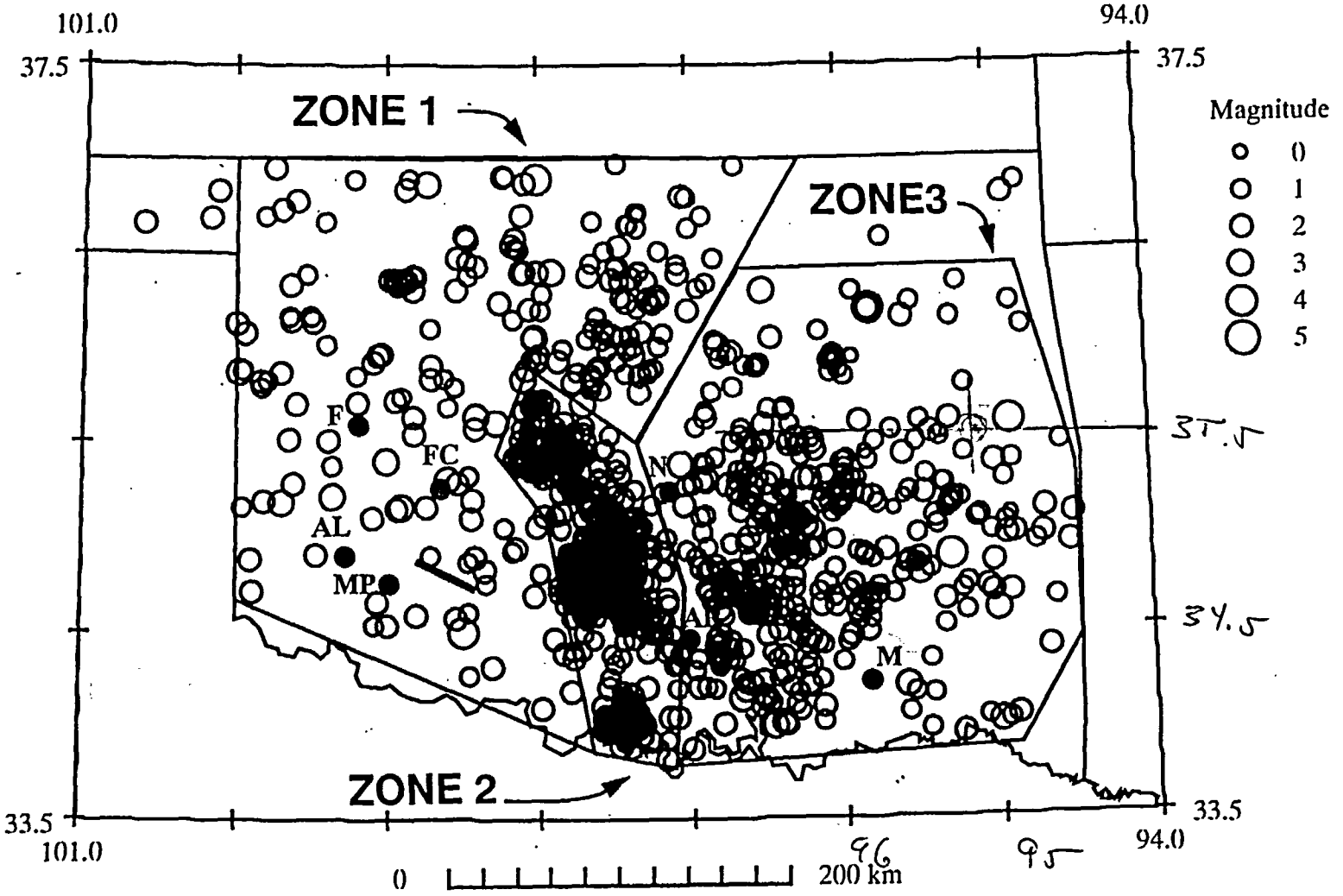

Figure 2-1. Central Oklahoma seismicity, 1987 - December 1996, and zonation boundaries. Dams are shown in red: **AR**=*Arbuckle,* **AL**=*Altus,* **F**=*Foss,* **FC**=*Fort Cobb,* **MP**=*Mountain Park,* **N**=*Norman,* **M**=*McGee Creek. Meers fault is shown in cyan.*

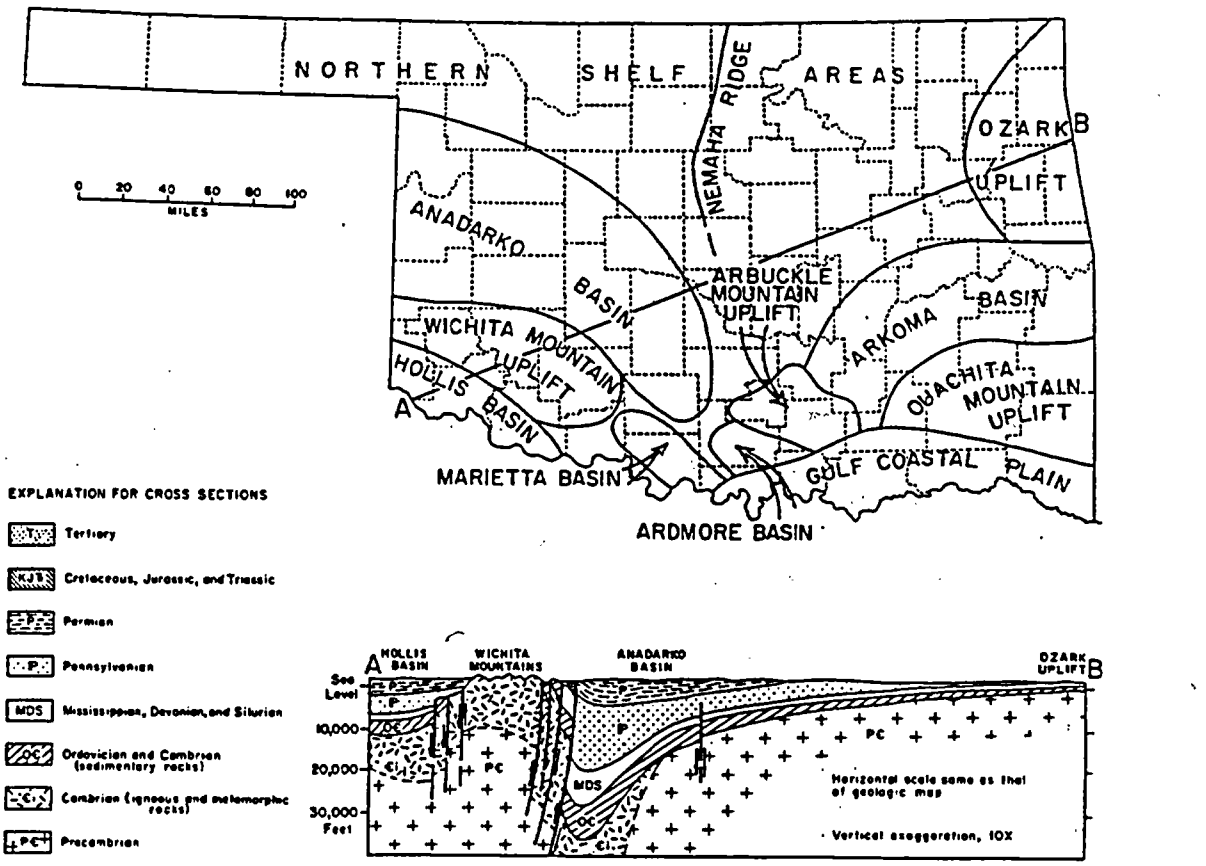

Figure 2-2. Major tectonic features of Oklahoma, from Luza and Lawson (1981).

We thus want to solve for t in the expression:

$$P(x > 0,t) = e^{-\lambda t}$$

where P is the probability level, x is the number of earthquakes in time t, and λ is 2/10,000. t can be equated to the return period, and $1/t$ the annual rate. For probability levels of .16, .50, and .84, the return periods are 9163, 3466, and 872 years, respectively. The $P = .50$ rate is close to the 4000 year return period used in developing the USGS National Hazard Maps (Frankel and others, 1966).

The Criner fault of southeastern Oklahoma was included in Geomatrix (1990) as a seismogenic feature. However, recent geologic investigations have indicated that it is not an active structure (Keith Kelson, personal communication, 1997).

In general, the seismicity distribution in figure 2-1 can be characterized by a low level of activity

in the western portion of the state, three areas of concentrated activity in the mid to south central portion, and a fairly uniform distribution in the southeastern region, apparently denser than the western region. Comparing figure 2-1 to figure 2-2, there appear to be no obvious relationships between tectonic features and seismicity patterns. The central clusters, however, lie between the Wichita Mountain and Ouachita Mountain Uplifts, and follow the eastern boundary of the Anadarko Basin. Whether this is physically significant or coincidence is not clear. Because detection capabilities in the state have been roughly uniform at about magnitude 2 and above since 1977 (J. Lawson, personal communication, 1997), the distribution shown in figure 2-1 is not significantly biased.

For the purposes of this study, the three zones of random seismicity shown in figure 2-1 were delineated. This zonation scheme is based purely on the appearance of recent seismicity, without regard to tectonic features, but is also influenced by the locations of the subject dams. Zone 1 consists of diffuse activity occurring in the western part of the study region. Zone 2 consists of three clusters of ongoing activity. The northernmost cluster contains the 1952 m_b 5.0 El Reno event. Zone 3 contains heterogeneous, diffuse seismicity. Not plotted, but included in the recurrence calculations for Zone 3, is a m_b 5.5 earthquake that occurred on October 22, 1882. This event has proven difficult to locate, but was most recently placed in eastern Oklahoma by Carlson (1984).

It has been suggested (Luza, 1985) that the central and southern clusters in Zone 2 are at least partly associated with petroleum extraction. However, an analysis designed to identify and quantify this possibility to our knowledge has not been conducted, and is beyond the scope of this report. Such a study would possibly lower the seismicity rates calculated for Zone 2.

2.3 Recurrence Calculations

2.3.1 Declustering

In order to compute earthquake recurrence for the three seismic source zones, it is necessary to delete aftershocks and other "dependent" events so that the catalog approximates a Poissonian, or random data set, estimate completeness periods for various magnitude ranges, and estimate the maximum magnitude of randomly occurring earthquakes.

In order to model and predict earthquake occurrence as a random process, the catalog must exhibit random space-time characteristics. However, due to the existence of foreshock-mainshock-aftershock sequences and swarms, the data set cannot be considered to have "random" or Poissonian characteristics. It was therefore necessary to identify and account for these events. The declustering algorithm of Reasenberg (1985) was used for this purpose. This technique, with some modifications, was used by Savage and DePolo (1993) to search for foreshocks in the Nevada seismicity catalog. The algorithm used in this report is based on these two papers, with some additional appropriate modifications. The major details are described below.

Any cluster identification scheme must establish criteria for deciding whether successive events in the catalog are "dependent" on or "independent" of neighboring ones in time and space. To determine spatial dependence, a "mainshock" is defined, with a magnitude-dependent source radius based on the circular crack model described in Kanamori and Anderson (1975) and a stress

drop of 30 bars. The radius of the next event in time is defined as its circular crack radius times a factor Q. If the distance between the two epicenters is less than the sum of the two radii, the two events are considered to be spatially dependent. Temporal dependence is judged by an application of Omori's Law, which describes the exponential decay of aftershocks with time. The aftershock sequence is modeled as a time-dependent Poisson process. The "look-ahead" time criterion is thus a function of the magnitude of the mainshock, the detection threshold magnitude, the confidence probability, and the time between the two events. Since the "look-ahead" time τ is proportional to the time difference, upper and lower bounds must be placed on it. If the time difference is less than τ, the two events are considered temporally dependent. If both spatial and temporal criteria are satisfied, the two events are considered dependent. If the magnitude of the second event exceeds that of the first, it is considered the new mainshock.

Because Reasenberg (1985) applied this technique to a catalog resulting from a spatially and temporally uniform seismograph network, he did not need to be concerned with changes in earthquake location capabilities through time. During the time span of our data set, however, (mid-1800's-1996) the changes in earthquake location precision have been great. Therefore it was necessary to place lower limits on the distance criteria, based on estimated relative epicentral location precision. These historical time-distance limits are shown in table 1. Estimated magnitude detection thresholds for these time periods are also shown in table 1. These values were used to estimate the maximum τ, as described in Savage and DePolo (1993). Minimum τ was set to 4 days, larger than the 1 day used by Reasenberg (1985) for a higher quality, lower magnitude data set. All other parameters used in the analysis were those recommended by Savage and DePolo (1993).

Table 2-1: Estimates of Maximum Epicentral Location Precision and Minimum Magnitude Used in Declustering Algorithm

Dates	Estimated Location Precision (km)	Minimum Magnitude
1/1850 - 12/1929	80	5.0
1/1930 - 12/1960	45	4.0
1/1962 - 12/1976	30	3.0
1/1977 - 12/1996	20	2.0

In lieu of available aftershock decay parameters for Oklahoma earthquakes, the parameters computed for a number of Utah Intermountain Seismic Belt earthquakes by Arabasz and Hill (1994) were used. The earthquakes in each identified cluster were combined into one "equivalent" event by finding the seismic moment-weighted average location and origin time. As opposed to computing an "equivalent" moment magnitude (based on the summed seismic moment) of all the events in the cluster, however, the largest magnitude of the cluster was used. Although some of the total seismic moment of the catalog is lost, magnitudes are not artificially inflated.

A plot of the declustered catalog, for events of magnitude 2 and greater, is shown in figure 2-3. Space-time diagrams for this data set are shown in figures 2-4a and b. The temporal behavior of

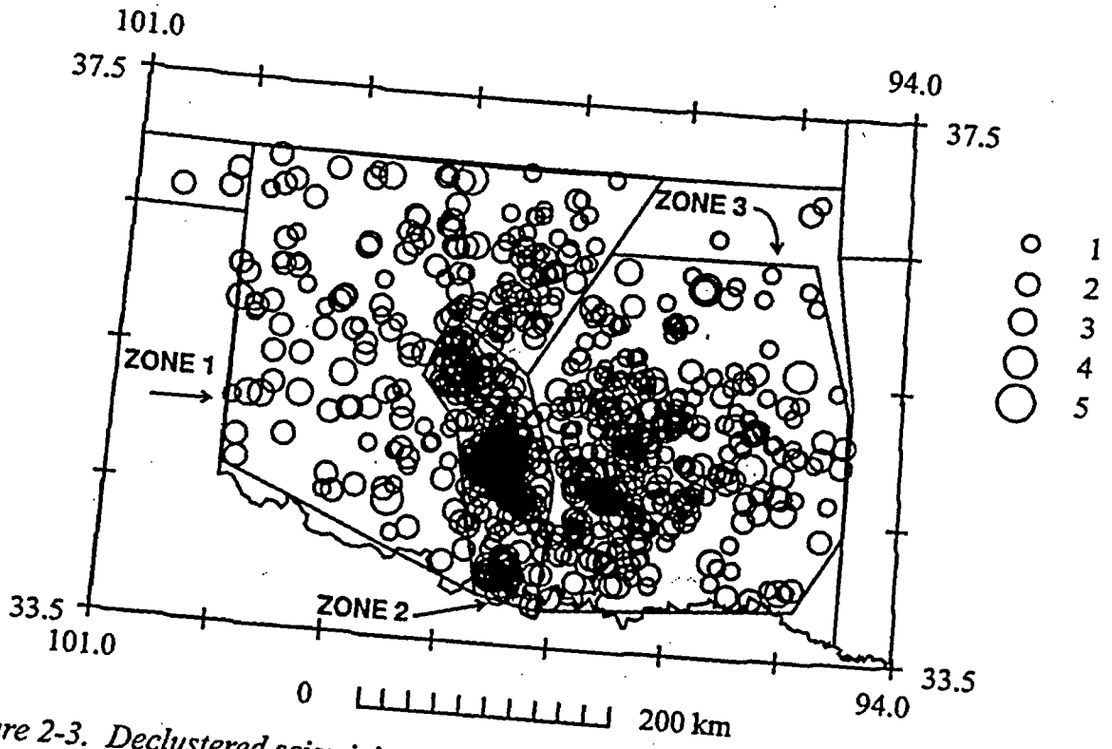

Figure 2-3. Declustered seismicity, magnitude 1 and greater.

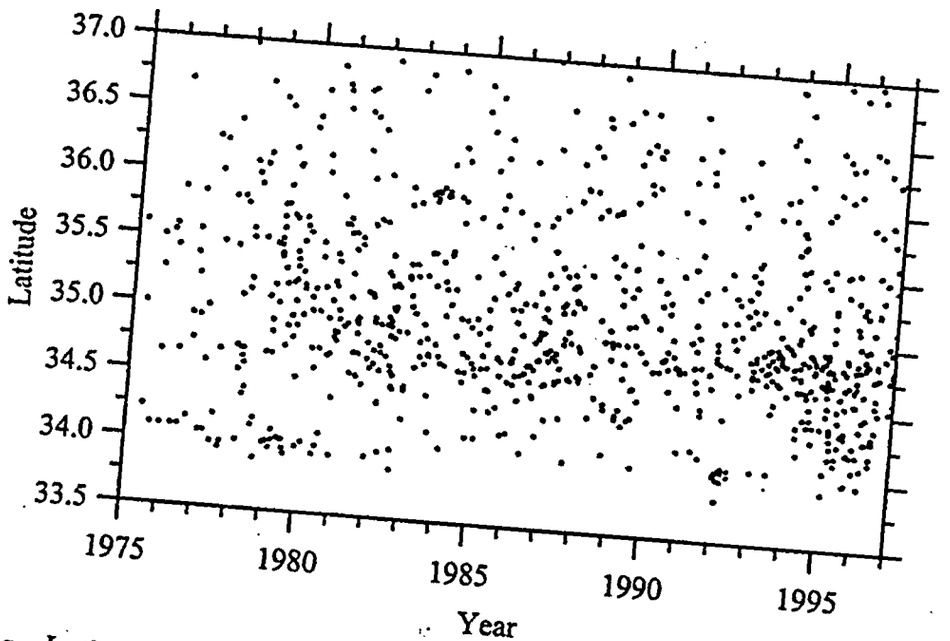

Figure 2-4a. Latitude vs. Time for earthquakes shown in figure 2-3.

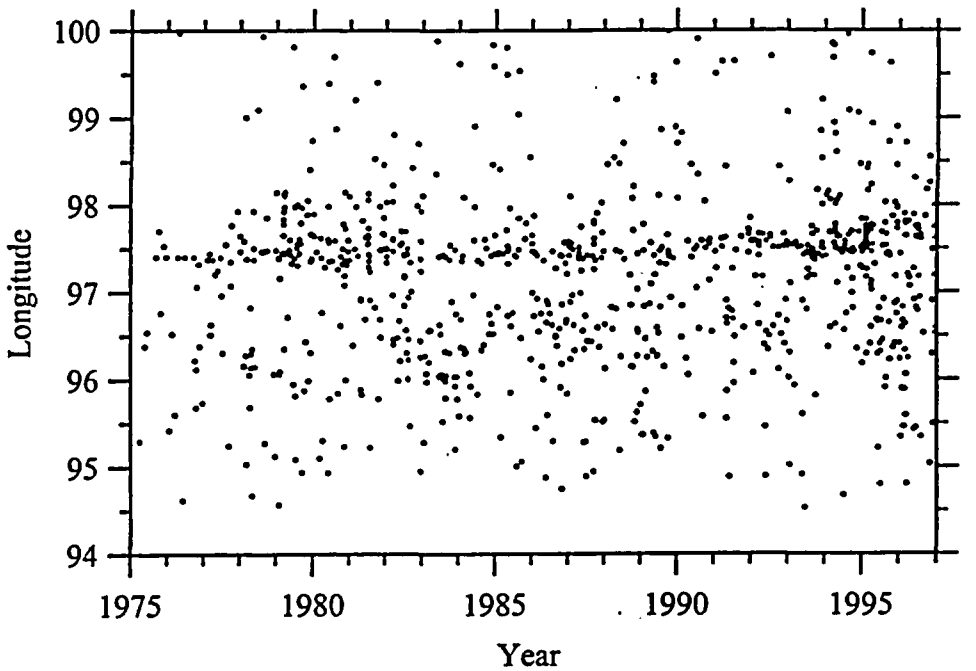

Figure 2-4b. Longitude vs. Time for earthquakes shown in figure 2-3.

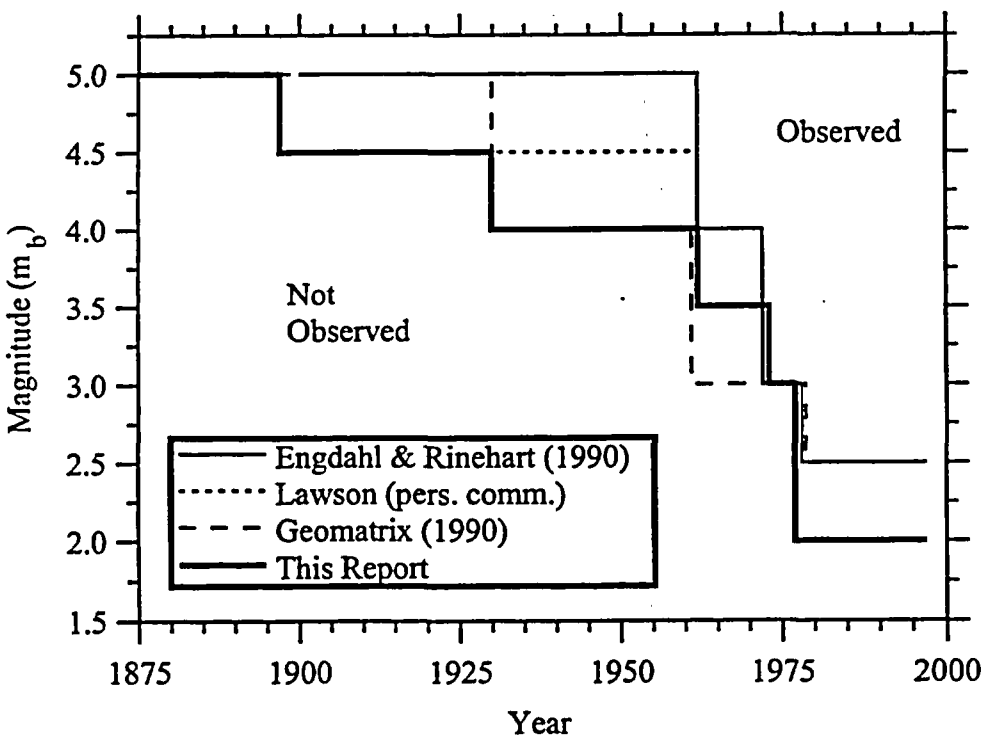

Figure 2-5. Completeness period estimates for Oklahoma from various sources, and those used in this report.

the three Zone 2 clusters is visible in these figures. The middle cluster at latitude 34.7 has been persistently active since at least 1978.

2.3.2 Completeness Periods

In order to compute earthquake recurrence it is necessary to estimate completeness periods for various magnitude ranges. Estimates for Oklahoma published or communicated by three sources are shown in graphical form in figure 2-5, in addition to the values adopted for this study. Note that the the J. Lawson curve is coincident with that used for this report below magnitude 3.5. Because seismograph station coverage in Zone 1 has been less dense than in the central and eastern parts of the state, the lowest detectable magnitude has been estimated to be 2.5. Table 2-2a gives the completeness period dates, and the number of earthquakes in each range for Zone 1 and table 2-2b gives the same information for Zones 2 and 3. The declustered earthquakes, filtered for these completeness periods, are plotted in figure 2-6.

Table 2-2a: Completeness Periods and Event Counts Used in Recurrence Calculations, Zone 1

Magnitude Range (m_b)	Completeness Period	Number of Earthquakes
		Zone 1
2.5 - 3.0	1/1977 - 12/1996	19
3.0- 3.5	1/1973 - 12/1996	6
3.5- 4.0	1/1962 - 12/1996	3
4.0 - 4.5	1/1930 - 12/1996	1
4.5 - 5.0	1/1897 - 12/1996	0
5.0 - 5.5	1/1850 - 12/1996	0
5.5 - 6.0	1/1850 - 12/1996	0

Table 2-2b: Completeness Periods and Event Counts Used in Recurrence Calculations, Zones 2 and 3

Magnitude Range (m_b)	Completeness Period	Number of Earthquakes	
		Zone 2	Zone 3
2.0 - 3.0	1/1977 - 12/1996	202	114
3.0- 4.0	1/1973 - 12/1996	8	2
4.0 - 5.0	1/1930 - 12/1996	2	4
5.0 - 6.0	1/1850 - 12/1996	1	1

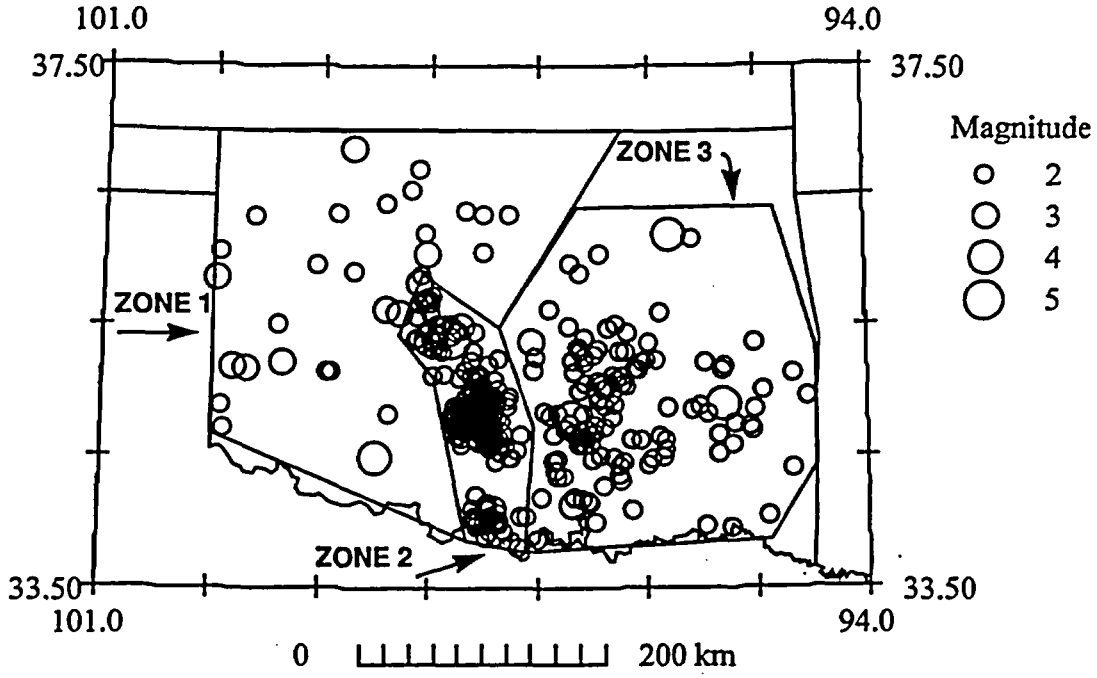

Figure 2-6. Earthquakes used in recurrence calculations.

2.3.3 Recurrence curves

Earthquake recurrence statistics were computed for each zone from this data set, using unequal observation periods for different magnitude ranges and the maximum likelihood method (Weichert, 1980). Data variances were computed as suggested in Weichert (1980). Model uncertainty bounds were calculated using the method of Bollinger and others (1989). Incremental recurrence curves for the three zones are shown in figures 2-7a, b, and c. Incremental curves, rather than cumulative, are shown because these rates and their uncertainties are those used in the probabilistic analysis. Tables 2-3a, b, and c give the computed and observed return periods for various magnitude ranges along with 95% confidence bounds, and table 2-4 gives the incremental and cumulative a and b recurrence parameters with their standard deviations. The a values have been normalized to events/year/km^2. The areas of the source zones are also given in table 2-4. Standard deviations for the Zone 3 cumulative parameters were not meaningful.

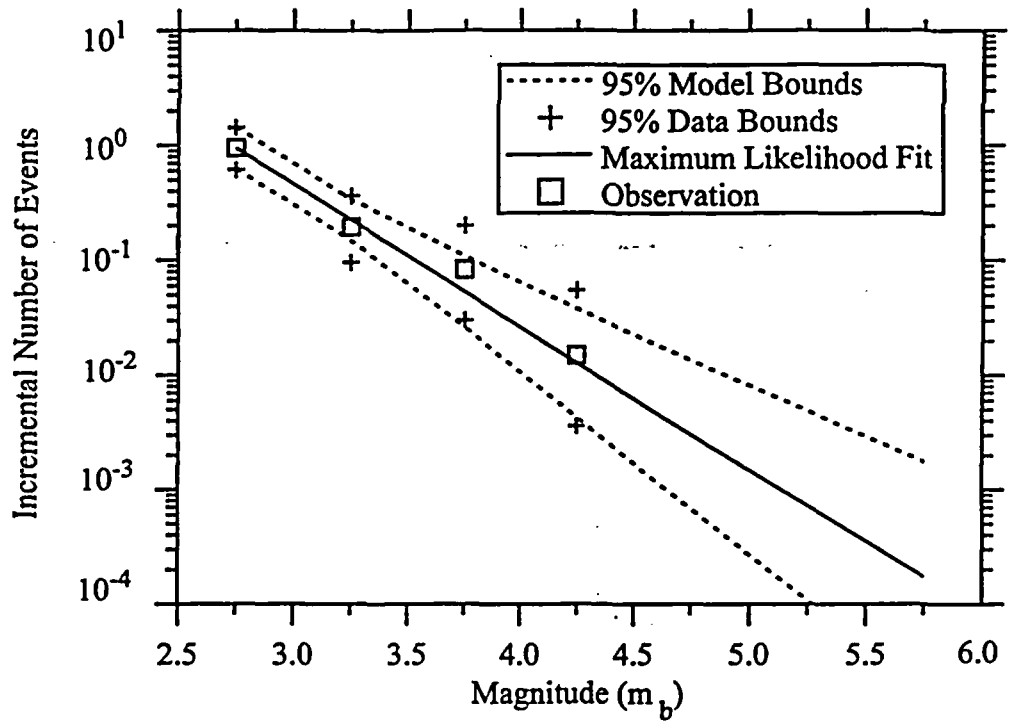

Figure 2-7a. Incremental recurrence curve for Zone 1.

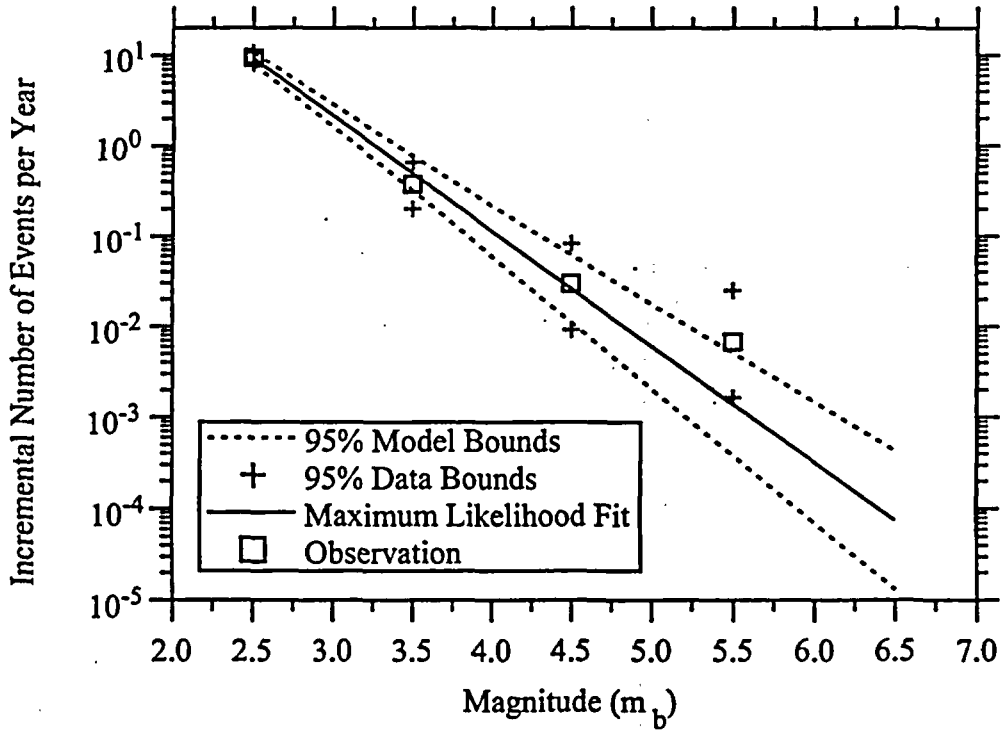

Figure 2-7b. Incremental recurrence curve for Zone 2.

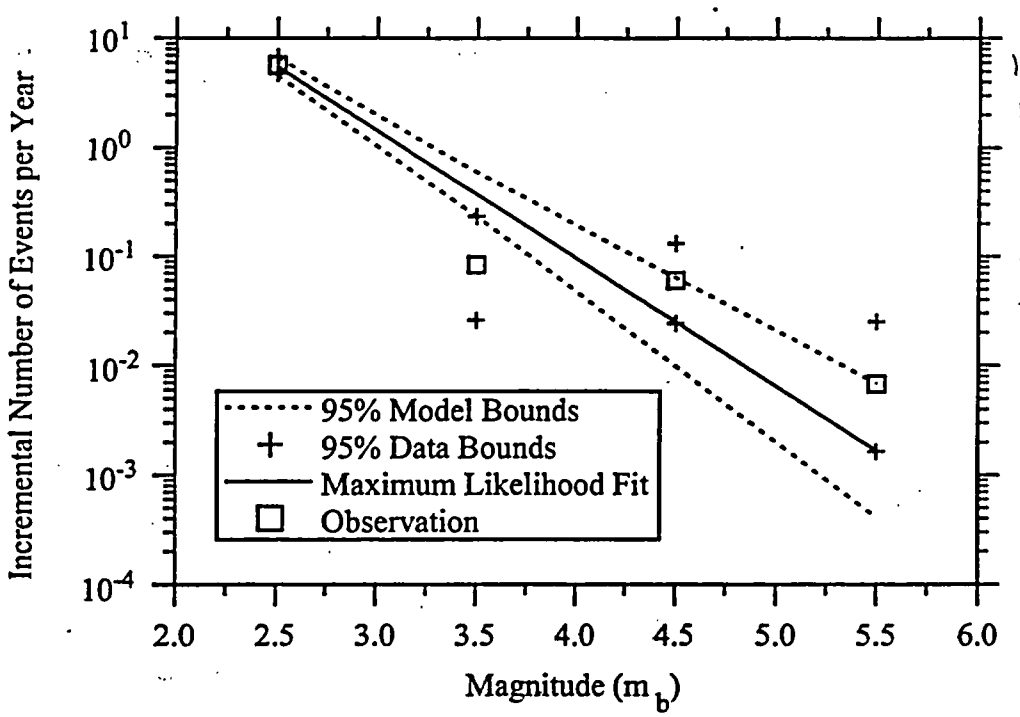

Figure 2-7c. Incremental recurrence curve for Zone 3.

Table 2-3a: Oklahoma Zone 1: Observed and Predicted Return Periods, with Upper and Lower Bounds of 95% Confidence Interval

Magnitude Range	Observed Return Period (yrs)	Predicted Return Period (yrs)	Lower Bound	Upper Bound
2.5 - 3.0	1.0	1.0	.67	1.5
3.0 - 3.5	4.0	4.2	2.8	6.3
3.5 - 4.0	12	17	8.6	34
4.0 - 4.5	67	70	25	197
4.5 - 5.0	not observed	285	69	1180
5.0 - 5.5	not observed	1170	192	7060
5.5 - 6.0	not observed	4770	535	42600

Table 2-3b: Oklahoma Zone 2: Observed and Predicted Return Periods, with Upper and Lower Bounds of 95% Confidence Interval

Magnitude Range	Observed Return Period (yrs)	Predicted Return Period (yrs)	Lower Bound	Upper Bound
2.0 - 3.0	.11	.11	.09	.12
3.0 - 4.0	2.7	2.0	1.3	3.1
4.0 - 5.0	34	38	16	90
5.0 - 6.0	147	716	195	2628
6.0 - 7.0	not observed	13,461	3135	76,750

Table 2-3c: Oklahoma Zone 3: Observed and Predicted Return Periods, with Upper and Lower Bounds of 95% Confidence Interval

Magnitude Range	Observed Return Period (yrs)	Predicted Return Period (yrs)	Lower Bound	Upper Bound
2.0 - 3.0	.18	.18	.15	.22
3.0 - 4.0	12	2.7	1.7	4
4.0 - 5.0	17	40	16	102
5.0 - 6.0	147	594	145	2430

Table 2-4: Recurrence Parameters for Random Seismicity Source Areas

	a, incremental (σ)	*a*, cumulative (σ)	*b* (σ; inc,cum)	Area (km^2)
Zone 1	-1.497 (.531)	-1.681 (.322)	1.124 (.174,.115)	71,778
Zone 2	-0.011 (.264)	-0.624(.384)	1.274 (.098,.183)	14,544
Zone 3	-1.145 (.282)	-1.701	1.172 (.107)	65,402

3.0 Probabilistic Seismic Hazard Analysis

3.1 Methodology and Inputs

A probabilistic seismic hazard analysis (PSHA) was performed for each damsite, using the random seismicity source zones and the Meers fault as seismic sources, as shown in figure 2-1. The basic methodology follows that of Cornell (1968). For the sources of randomly occurring seismicity, a gridded point-source model was used to distribute seismicity uniformly in the source regions. The grid spacing was 5 km.

The Meers fault was modeled as a line source using the program SEISRISK III (Bender and Perkins, 1987). Assigned activity rates and return periods for the 16th, 50th, and 84th percentile levels are developed in section 2.2. It is assumed that the fault is capable of producing only M_W 7.0 earthquakes.

The Quaternary history of the Meers fault consists of two Holocene events, preceded by several hundred thousand years of quiescence. This raises the question of whether the the fault is in an "active" phase, with return periods for surface faulting events on the order of several hundred to a few thousand years, or whether it will remain dormant for the next several hundred thousand years or more. There is little, if any, scientific information to support either scenario. For this study it is judged that there is a 70% probability that the Meers fault will continue to be active at the Holocene rate for the life of the dams.

Two ground motion attenuation functions, EPRI (1993) and Atkinson and Boore (1995), were used in the analysis. Both are based on the stochastic point source modeling technique, with input parameters and results constrained by the meager collection of records available for eastern North America (The EPRI (1993) relation also used two western North America events for calibration purposes). A comparison of the two relations is found in Atkinson and Boore (1997). The Atkinson and Boore (1995) relation in general gives higher median PHA results due to the assumption of less high-frequency attenuation. The EPRI (1993) relation uses horizontal distance to the surface projection of the fault as its distance measure, equivalent to the Joyner-Boore distance (e.g., Joyner and Boore, 1988) and "fictitious" depths. Atkinson and Boore (1997) assumed a hypocentral depth of 10 km in developing their relation.

A third eastern North America relation has been developed by Frankel and others (1996), and gives results very similar to EPRI (1993) (Atkinson and Boore, 1997). For the purposes of this study, the EPRI (1993) relation was given a weight of .67; the Atkinson and Boore (1995) relation by .33. The reasons for preferring the EPRI (1993) relation are its similarity to the Frankel and others (1996) relation, and that Atkinson and Boore (1995) express little confidence in their peak horizontal acceleration results. The EPRI (1993) relation also contains more detailed uncertainty calculations; these have a significant impact on the final results.

Uncertainties in attenuation and seismicity rate were accounted for by complete enumeration. The lognormal probability density functions (PDFs) for each parameter were discretized into 50 equal-probability values, resulting in 2500 models. The results from these models were then ordered and integrated into PDFs for each acceleration exceedance level. Formal Gaussian seis-

micity (log) rate uncertainties were calculated as part of the earthquake recurrence computations, and are represented by 95th percentile confidence bounds in figures 2-7a-c. Ground motion uncertainties as described in the attenuation relation documentation were applied. The EPRI (1993) uncertainties are described in Toro and others (1997), and are frequency, magnitude, and distance dependent. The Atkinson and Boore (1995) uncertainties are only frequency dependent. Because no standard deviation was listed for peak horizontal acceleration, their value for 10 hz spectral response was used.

It is necessary to estimate maximum magnitudes for each random source zone for use in the probabilistic analysis. This is perhaps the most difficult task of seismic hazard assessment. A number of approaches can be taken, all of which rely on poor circumstantial evidence (e.g., EPRI, 1987).

Two comprehensive seismic hazard studies were conducted during the 1980s for the central and eastern U.S., one by the Electric Power Research Institute (EPRI, 1986) and the other by Lawrence Livermore National Laboratory for the Nuclear Regulatory Commission (Bernreuter and others, 1989). Both relied heavily on zonation and maximum magnitude estimates made by experts. Table 3-1 lists the estimates of maximum magnitude (m_b) made in these studies for their corresponding source region. Because the source zones in these studies rarely coincided exactly with those used here, judgement was exercized in correlating zones. In some cases a weighted average of magnitudes as presented in the studies was calculated; in others an average of two zones was taken if they were contained in the zones used in this study. In addition, estimates from two other reports or articles are presented.

Taking the mean of the estimates resulted in m_b 6.1 for Zone 1, m_b 6.3 for Zone 2, and m_b 6.0 for Zone 3. Values adopted for this study were m_b 6.0 for Zone 1, m_b 6.5 for Zone 2, and m_b 6.0 for Zone 3. A minimum magnitude of 5.5 was also applied. It was judged that events of magnitudes less than 5.5 are not of engineering significance to the dams.

Table 3-1: Estimates of Maximum Magnitude (m_b) from Available Publications

Source	Zone 1	Zone 2	Zone 3
Bernreuter and others (1989) Expert 2	6.0	6.5, 6.5, 7.0	6.5
Bernreuter and others (1989) Expert 3	6.0	6.0	5.5
Bernreuter and others (1989) Expert 4		6.1	5.6
Bernreuter and others (1989) Expert 6	6.8	6.8	6.8
Bernreuter and others (1989) Expert 7	6.5	6.5	6.5
Bernreuter and others (1989) Expert 10	6.3	6.3	6.3
Bernreuter and others (1989) Expert 11	6.5	6.5	6.5
Bernreuter and others (1989) Expert 12	6.0	6.0	6.0
EPRI (1987), Vol. 5		5.9	

Table 3-1: Estimates of Maximum Magnitude (m_b) from Available Publications

Source	Zone 1	Zone 2	Zone 3
EPRI (1987), Vol. 6	6.0	6.2	5.3
EPRI (1987), Vol. 7	6.1	5.7	5.5
EPRI (1987), Vol. 9	5.9	6.8	5.9
Nuttli and Herrmann (1978)	6.3	6.3	6.3
Johnston and Nava (1990)	5.3	6.0	5.3
Mean of the Above:	6.1	6.3	6.0
This Study	6.0	6.5	6.0

A logic tree computation scheme was applied, based on the weights given the two attenuation relations and the estimated probability of activity on the Meers fault. This structure, with the assigned probabilities, is shown in figure 3-1.

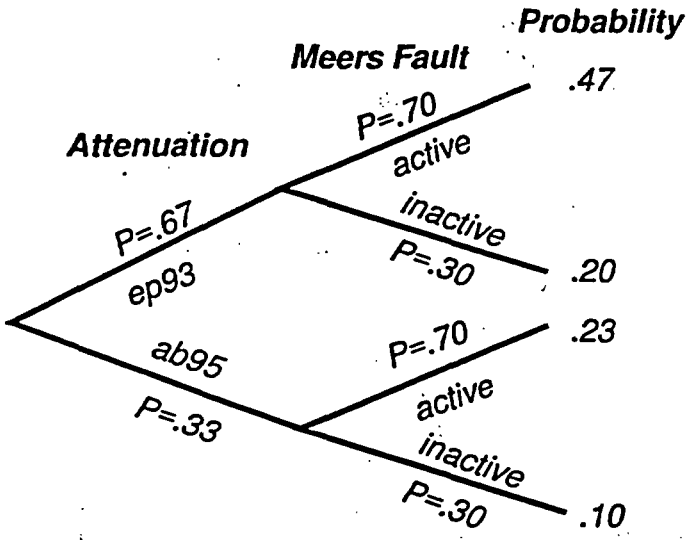

Figure 3-1. Logic tree of attenuation relation choices and Meers fault activity. ep93 refers to EPRI (1993); ab95 refers to Atkinson and Boore (1995).

3.2 Results

Ground motion results are presented in the form of hazard curves for Peak Horizontal Acceleration (PHA), Uniform Hazard Spectra (UHS) for return periods of 10,000 and 50,000 years, and ASI and VSI (von Thun and others, 1988) for the two return periods. 16th, 50th (mean), and 84th percentile results are shown. The results are presented in Appendices A through G, corresponding to results for Altus, Arbuckle, Fort Cobb, Foss, McGee Creek, Mountain Park, and Norman Dams, respectively.

A description of the figures and table in each appendix is as follows:

Figure 1 shows PHA hazard curves for all relevant sources (individual random sources and the Meers fault) and the cumulative curve, for the EPRI (1993) attenuation relation. The relevant sources are different for each dam, depending on its geographic location in relation to the seismic sources.

Figure 2 is the same as figure 1, except that results for the Boore and Atkinson (1995) attenuation relation are shown.

Figure 3 is the final PHA hazard curve calculated according to the logic tree shown in figure 3-1, for the 16th, 50th (mean), and 84th percentile levels.

Figure 4 shows Uniform Hazard Spectra (UHS) for a 10,000 year return period, for the random earthquake and Meers fault source, for each attenuation relation.

Figure 5 is the same as figure 4, but for a 50,000 year return period.

Figure 6 shows the final UHS for a 10,000 year return period, at the 16th, 50th (mean), and 84th percentile levels.

Figure 7 is the same as figure 6, but for a 50,000 year return period.

Table 1 gives PHA, ASI, and VSI results for the two return periods, at the 16th, 50th (mean), and 84th percentile levels.

3.3 Discussion

The PHA hazard curves reflect their proximity to the various seismic sources. The Meers fault is the dominant source for Mountain Park and Fort Cobb dams, which lie at distances of 33 and 37 km, respectively, from the fault. For these sites, the hazard from the Meers fault exceeds that from the random seismicity. For Altus Dam, at 58 km, the hazards from the fault and random seismicity source are approximately equal. For the remaining dams, the fault assumes diminishing significance with distance. Ground motions levels at McGee Creek Dam, 223 km from the fault, were less than .01 g at all spectral response periods, and are therefore not portrayed. Proximity to Zone 2 (Arbuckle and Norman dams) produces relatively high values, due to its higher rate of activity and higher maximum magnitude, relative to Zones 1 and 3.

Proximity to the Meers fault is also reflected in the shapes of the uniform hazard spectra. For example, the PHA hazard curves for Fort Cobb and Norman dams are relatively high compared to the others. Fort Cobb dam is fairly close to the Meers fault, and Norman dam is close to Zone 2, which has the highest level of seismicity of the three zones, and also the highest maximum magnitude. However, at longer periods the responses for Fort Cobb dam are higher than for Norman Dam. This is because M_W 7 events on the Meers fault generate higher amplitude long period motion than Zone 2 events, which consist of earthquakes in the m_b 5.5 to 6.5 range.

Finally, it is necessary to point out that estimates of peak acceleration critically depend on regional high frequency attenuation, a little-known parameter in eastern North America. Atkinson and Boore (1995), in discussing their attenuation relation, state that "...we assume that frequencies above 20 Hz *(including peak acceleration)* are not of engineering interest". Consequently, the response spectra developed in this report constitute a more reliable and meaningful characterization of the seismic hazard than peak horizontal acceleration.

4.0 References

Arabasz, W.J. and S.J. Hill (1994), Progress Report for 1993 on: Aftershock temporal behavior and earthquake clustering in the Utah region, University of Utah Seismograph Stations, University of Utah, 31 pp.

Atkinson, G.M., and D.M. Boore (1995), Ground motion relations for eastern North America, Bulletin of the Seismological Society of America, 85, 17-31.

Atkinson, G.M., and D.M. Boore (1997), Some comparisons between recent ground motion relations, Seismological Research Letters, 68, no. 1, 24-41.

Bender, B., and D.M. Perkins (1989), SEISRISK III, a computer program for seismic hazard estimation, U.S. Geological Survey Bulletin 1772, 48 pp.

Bernreuter, D.L., J.B. Savy, R.W. Mensing, and J.C. Chen (1989), Seismic hazard characterization of 69 nuclear power plant sites east of the Rocky Mountains, U.S. Nuclear Regulatory Commission, NUREG/CR-5250.

Bollinger, G.A., F.C. Davison, M.S. Sibol, and J.B. Birch (1989), Magnitude recurrence relations for the southeastern United States and its subdivisions, Journal of Geophysical Research, 94, 2857-2873.

Carlson, S.M. (1984), Investigations of recent and historical seismicity in east Texas, M.A. Thesis, University of Texas, Austin.

Cornell, C.A. (1968), Engineering seismic risk analysis, Bulletin of the Seismological Society of America, 58, 1583-1606.

Crone, A.J., and K.V. Luza (1990), Style and timing of Holocene surface faulting on the Meers fault, southwestern Oklahoma, Geological Society of America Bulletin, 102, 1-17.

Donovan, R.N., M.C. Gilbert, K.V. Luza, D. Marchini, and D. Sanderson (1983), Possible Quaternary movement on the Meers fault, southwestern Oklahoma, Oklahoma Geology Notes, 43, no. 5, 124-133.

Engdahl, E.R., and W.A. Rinehart (1991), Seismicity Map of North America Project, in: Slemmons, D.B., Engdahl, E.R., Zoback, M.D., and Blackwell, D.D., eds., Neotectonics of North America: Boulder, Colorado, Geological Society of America, Decade Map Volume 1.

EPRI (Electric Power Research Institute) (1986), Seismic hazard methodology for the central and eastern United States, EPRI NP-4726.

EPRI (1987), Methods for assessing maximum earthquakes in the Central and Eastern United States, Electric Power Research Institute, EPRI RP2556-12.

EPRI (1993), Guidelines for determining design basis ground motions, vol. 1, EPRI TR-102293.

Frankel, A., C. Mueller, T. Barnhard, D. Perkins, E. Leyendecker, N. Dickman, S. Hanson, and M. Hopper (1996), National seismic-hazard maps: documentation June 1966, U.S. Geological Survey Open-File Report 96-532.

Geomatrix Consultants (1990), Seismotectonic evaluation, Wichita Uplift region, southern Oklahoma and northern Texas, Report for U.S. Bureau of Reclamation, 113 pp.

Harlton, B.H. (1963), Frontal Wichita fault system of southwestern Oklahoma, American Association of Petroleum Geologists Bulletin, 47, no. 8, 1552-1580.

Hildebrand, G.M., D.W. Steeples, R.W. Knapp, R.D. Miller, and B.C. Bennett (1988). Microearthquakes in Kansas and Nebraska 1977-1987, Seismological Research Letters, 59, no. 4, 159-165.

Johnston, A.C. and S.J. Nava (1990), Seismic-hazard assessment in the central United States, *in* Krinitzsky, E.L., and Slemmons, D.B., Neotectonics in earthquake evaluation, Geological Society of America Reviews in Engineering Geology, v. 8, 47-58.

Joyner, W.B., and D.M. Boore (1988), Measurement, characteristics and prediction of strong ground motion, Proceedings, Specialty Conference on Earthquake Engineering and Soil Dynamics II, ASCE, Park City, Utah, 43-102.

Kanamori, H., and D.L. Anderson (1975), Theoretical basis for some empirical relations is seismology, Bulletin of the Seismological Society of America, 65, 1073-1079.

Lawson, J.E. (1985), Expected earthquake ground-motion parameters at the Arcadia, Oklahoma, dam site, Oklahoma Geological Survey Special Publication 85-1, 41 pp.

Luza, K.V. and J.E. Lawson (1981), Seismicity and tectonic relationships of the Nemaha Uplift in Oklahoma, Part IV, U.S. Nuclear Regulatory Commission, NUREG/CR-2439.

Luza, K.V. and J.E. Lawson (1983), Seismicity and tectonic relationships of the Nemaha Uplift in Oklahoma, Part V (Final Report), U.S. Nuclear Regulatory Commission, NUREG61 CR-3109.

Luza, K.V. (1985), Oklahoma, in Seismicity and tectonic relationships of the Nemaha uplift and midcontinent geophysical anomaly (Final Project Summary), Oklahoma Geological Survey Special Publication 85-2, 14-20.

Nuttli, O.W. and R.B. Herrmann (1978), Credible earthquakes for the central United States, U.S. Army Engineer Waterways Experiment Station, Vicksburg, Mississippi, Report 12.

Ramelli, A.R. (1988), Late Quaternary tectonic activity of the Meers fault, southwest Oklahoma, M.S. thesis, University of Nevada, Reno, Nevada, 123 pp.

Reasenberg, P. (1985), Second-order moment of central California seismicity, 1969-1982, Journal of Geophysical Research, 90, 5479-5495.

Savage, M.K., and D.M. DePolo (1993), Foreshock probabilities in the western Great Basin-eastern Sierra Nevada, Bulletin of the Seismological Society of America, 83, 1910-1939.

Swan, F.H., J.R. Wesling, K.A. Hanson, K.I. Kelson, and R.C. Perman (1993), Investigation of the Quaternary structural and tectonic character of the Meers fault, southwestern Oklahoma, Draft Report for U.S. Nuclear Regulatory Commission, NRC-04-87-007, Geomatrix Consultants, 104 pp.

Toro, G.R., N.A. Abrahamson, and J.F. Schneider (1997), Model of strong ground motions from earthquakes in central and eastern North America: best estimates and uncertainties, Seismological Research Letter, 68, no. 1, 41-58.

von Thun, J.L., L.H. Roehm, G.S. Scott, and J.A. Wilson (1988), Earthquake ground motions for design and analysis of dams, in: Proceedings of Earthquake Engineering and Soil Dynamics II, Park City, Utah, GT Div/ASCE, 463-482.

Weichert, D. (1980), Estimation of the earthquake recurrence parameters for unequal observation periods for different magnitudes, Bulletin of the Seismological Society of America, 70, 1337-1347.

Appendix E

Results for McGee Creek Dam

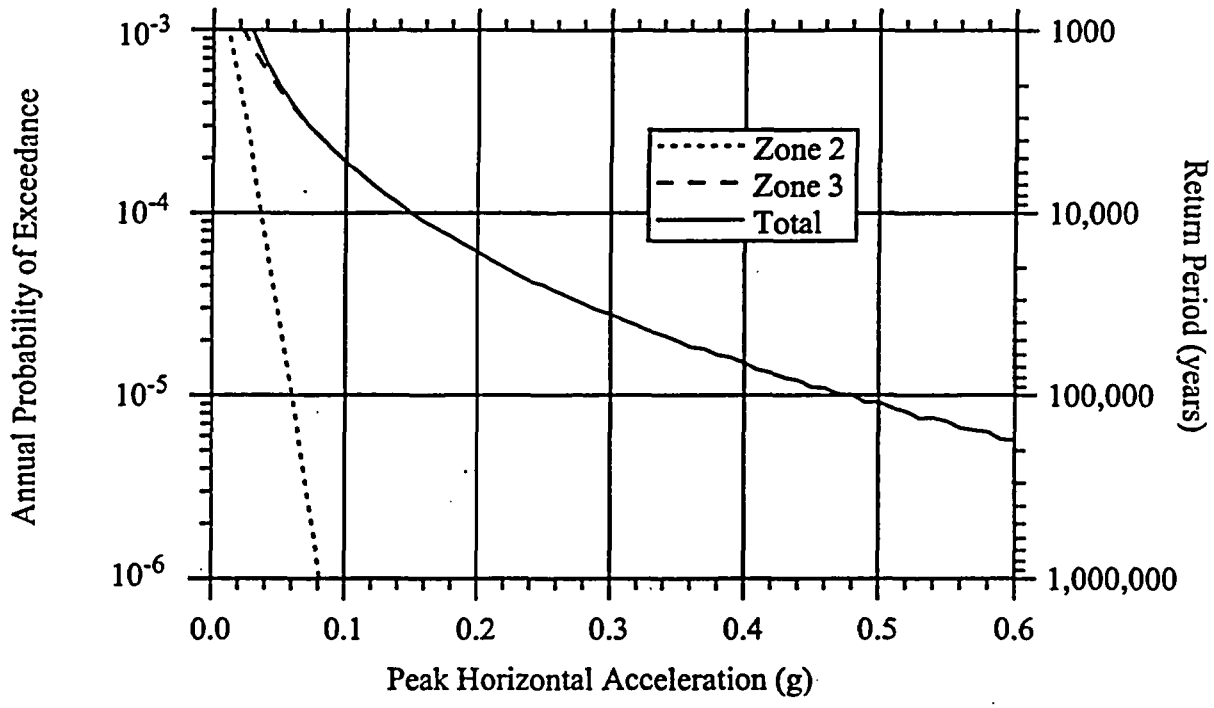

Figure E-1. McGee Creek Dam: individual and total hazard curves for PHA, EPRI (1993) attenuation.

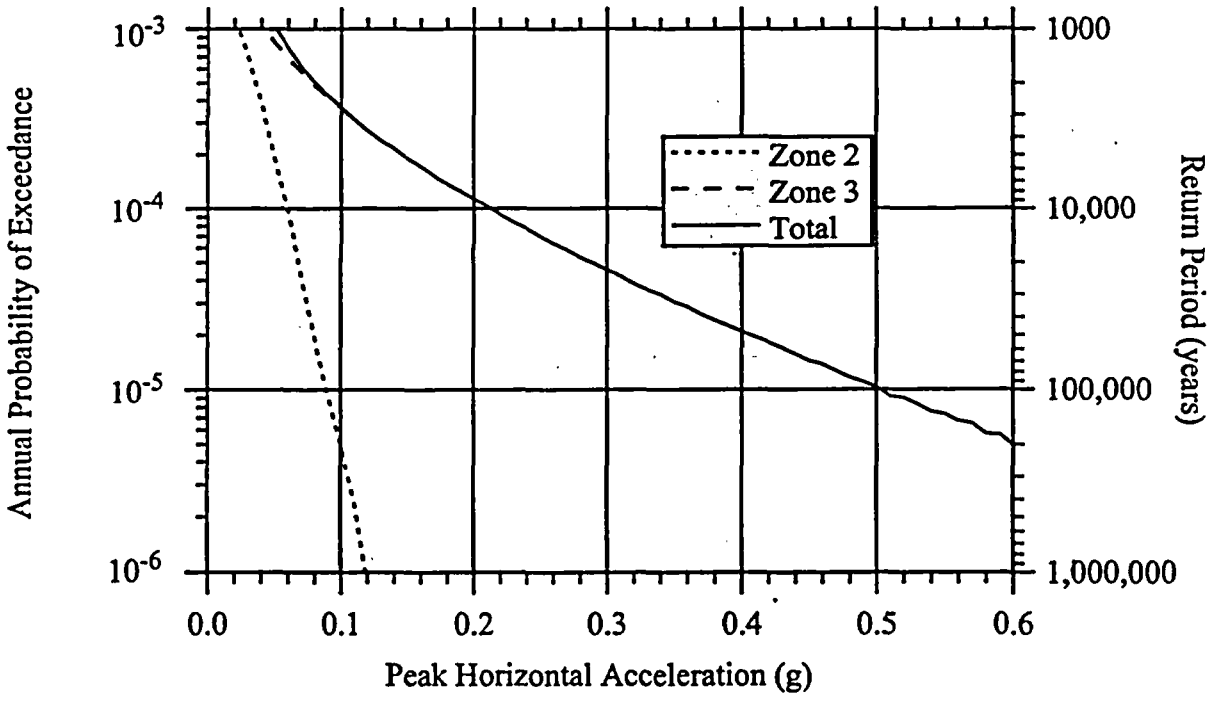

Figure E-2. McGee Creek Dam: individual and total hazard curves for PHA, Atkinson and Boore (1995) attenuation.

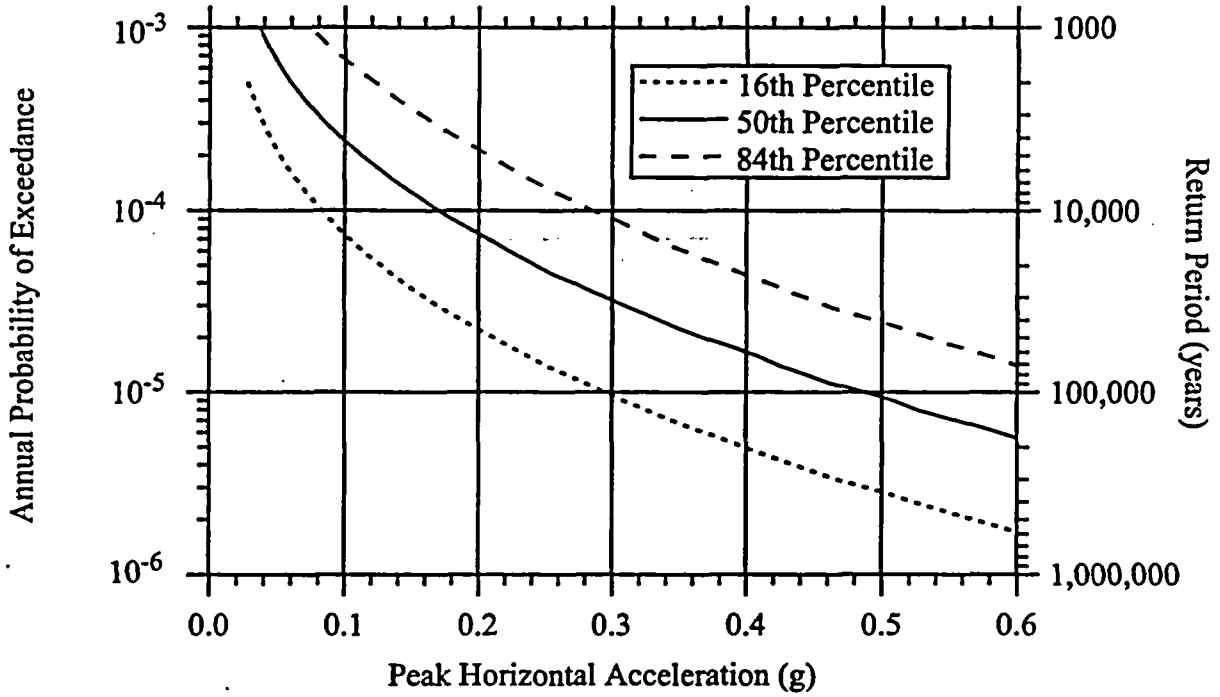

Figure E-3. McGee Creek Dam: Final PHA hazard curves.

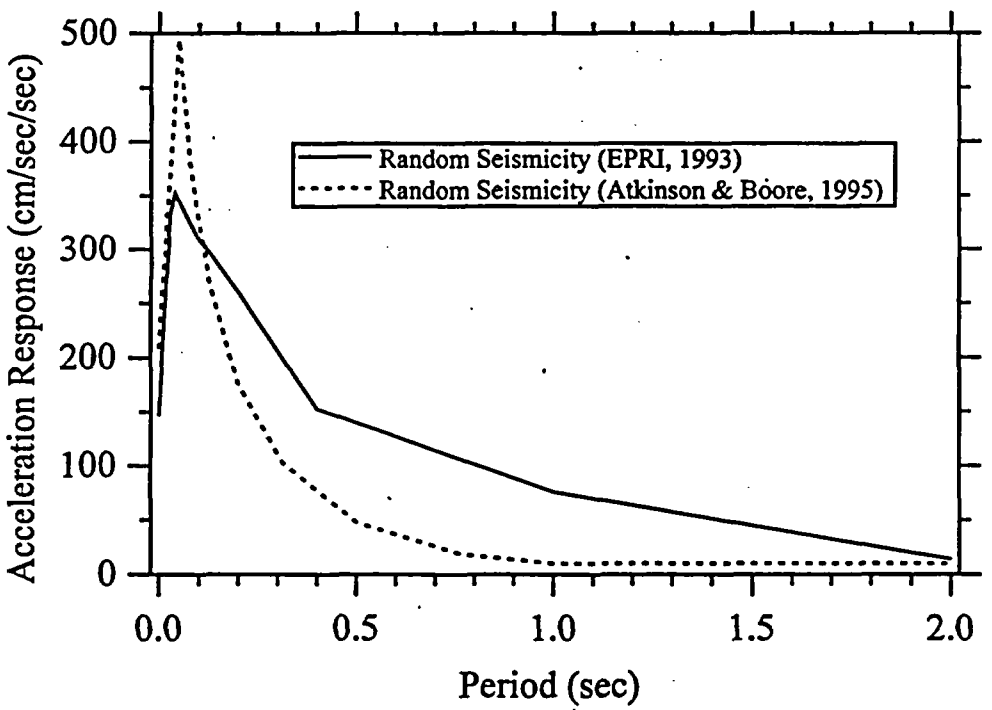

Figure E-4. McGee Creek Dam: Uniform hazard acceleration response spectra for random seismicity, return period of 10,000 years.

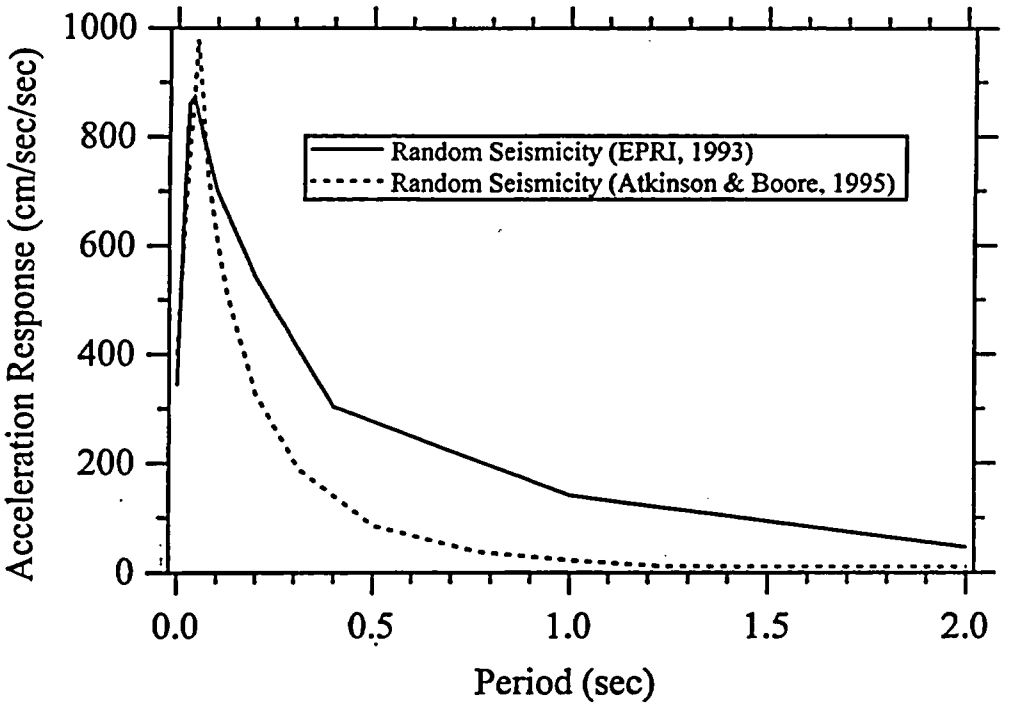

Figure E-5. McGee Creek Dam: Uniform hazard acceleration response spectra for random seismicity, return period of 50,000 years.

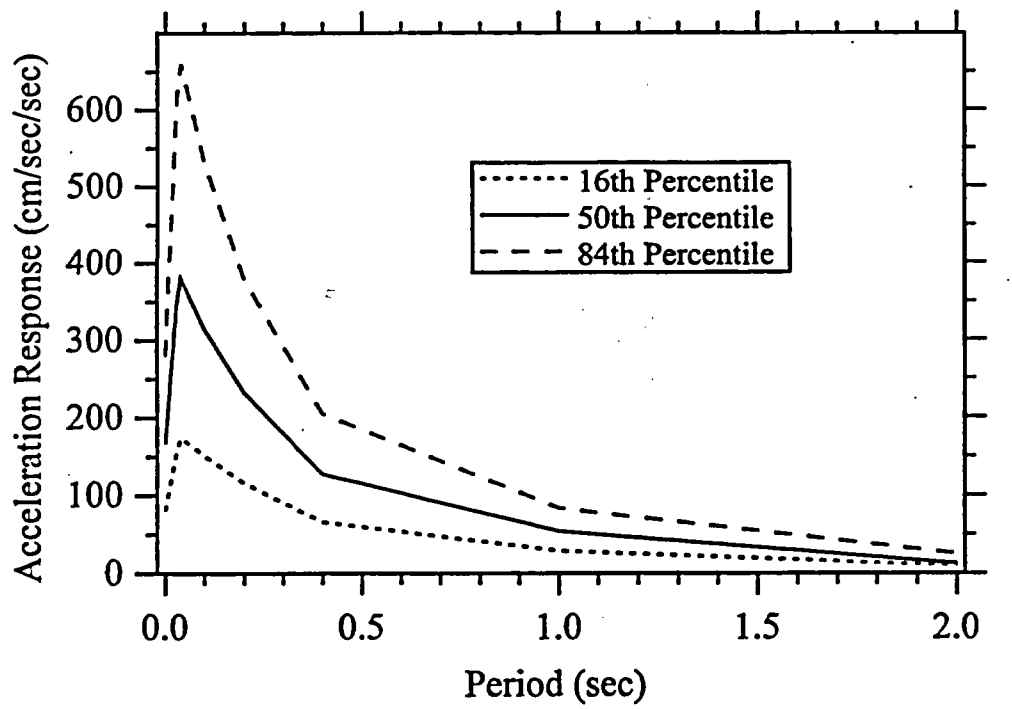

Figure E-6. McGee Creek Dam: Final acceleration response spectra, for return period of 10,000 years.

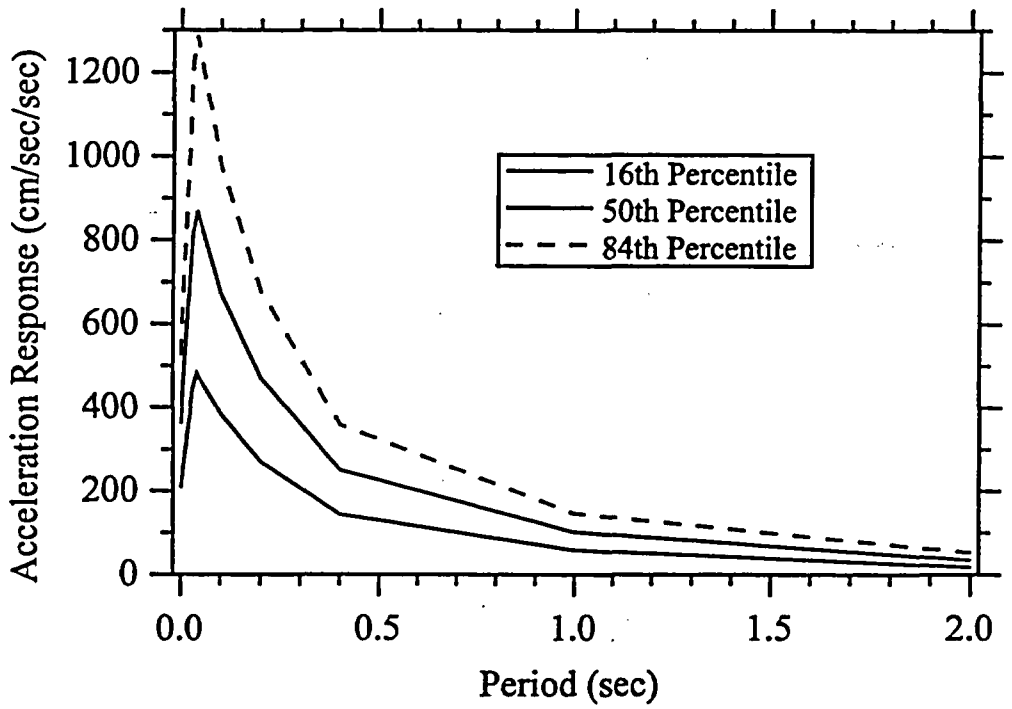

Figure E-7. McGee Creek Dam: Final acceleration response spectra, for return period of 50,000 years.

Table E-1
Summary Results for McGee Creek Dam

Percentile	PHA (g)		ASI (cm/sec)		VSI (cm)	
	10,000 yrs	50,000 yrs	10,000 yrs	50,000 yrs	10,000 yrs	50,000 yrs
16th	.08	.21	69	156	8	16
50th	.17	.37	136	272	14	28
84th	.29	.53	221	391	22	40

Initial Draft
10/5/04

Comprehensive Facility Review
McGee Creek Dam
Seismic Hazard

I. Seismic Hazard

McGee Creek Dam is located in southeastern Oklahoma. Historic seismicity within the state has been relatively low, the two largest events being a m_b 5.5 event somewhere in the Oklahoma-Missouri boundary region in 1882, and a m_b 5.0 event near El Reno (seen in the upper part of Zone 2 in Figure 1) in 1952. The Meers fault lies about 230 km WNW of the Dam, and has apparently produced two surface faulting events in the past 10,000 years. Potential magnitudes for the Meers fault have be estimated to be in the 6.75 to 7.25 range; however, due to its distance from McGee Creek Dam, it is not considered in the hazard analysis.

Seismic loadings for McGee Creek Dam have been updated from LaForge [1], and the reader is referred to that document for more complete information. Seismicity was updated through September, 2004, and advances in computational techniques since the 1997 study were implemented.

Figure 1 shows the location of McGee Creek Dam, the Meers fault, and seismicity used in the hazard calculations. Seismicity was divided into three areal zones, based on observations of all historic seismicity. From the seismic hazard standpoint, the dam is affected only by seismicity in Zone 3. However, due to the small number (7) of earthquakes of magnitude 3 or greater in this zone (the 1882 event is not plotted in Figure 1) recurrence was computed for all three zones, and this rate applied to sites in Zone 3. While the total number of events used (33) provides a much more stable estimate of seismicity rates, hazard estimates for Zone 3 will be on the conservative side.

Figure 2 shows the mean hazard curve for PHA, with fractiles. The PHA levels for return periods of 5000, 10,000 and 50,000 years are 0.11 g, 0.15 g, and 0.33 g, respectively. Mean uniform hazard response spectra (UHS) are shown in Figure 3.

II. Strong-Motion Monitoring

There are no strong-motion instruments at McGee Creek Dam, and no significant earthquakes have occurred in area since it was constructed.

Initial Draft
9/28/04/04

Reference

[1] "Seismic Hazard and Ground Motion Analysis for Altus, McGee Creek, Fort Cobb, Foss, McGee Creek, Mountain Park, and Norman Dams", *Seismotectonic Report 7-1*, prepared by Roland LaForge, U.S. Bureau of Reclamation, Denver, Colorado, 19 p., 1997.

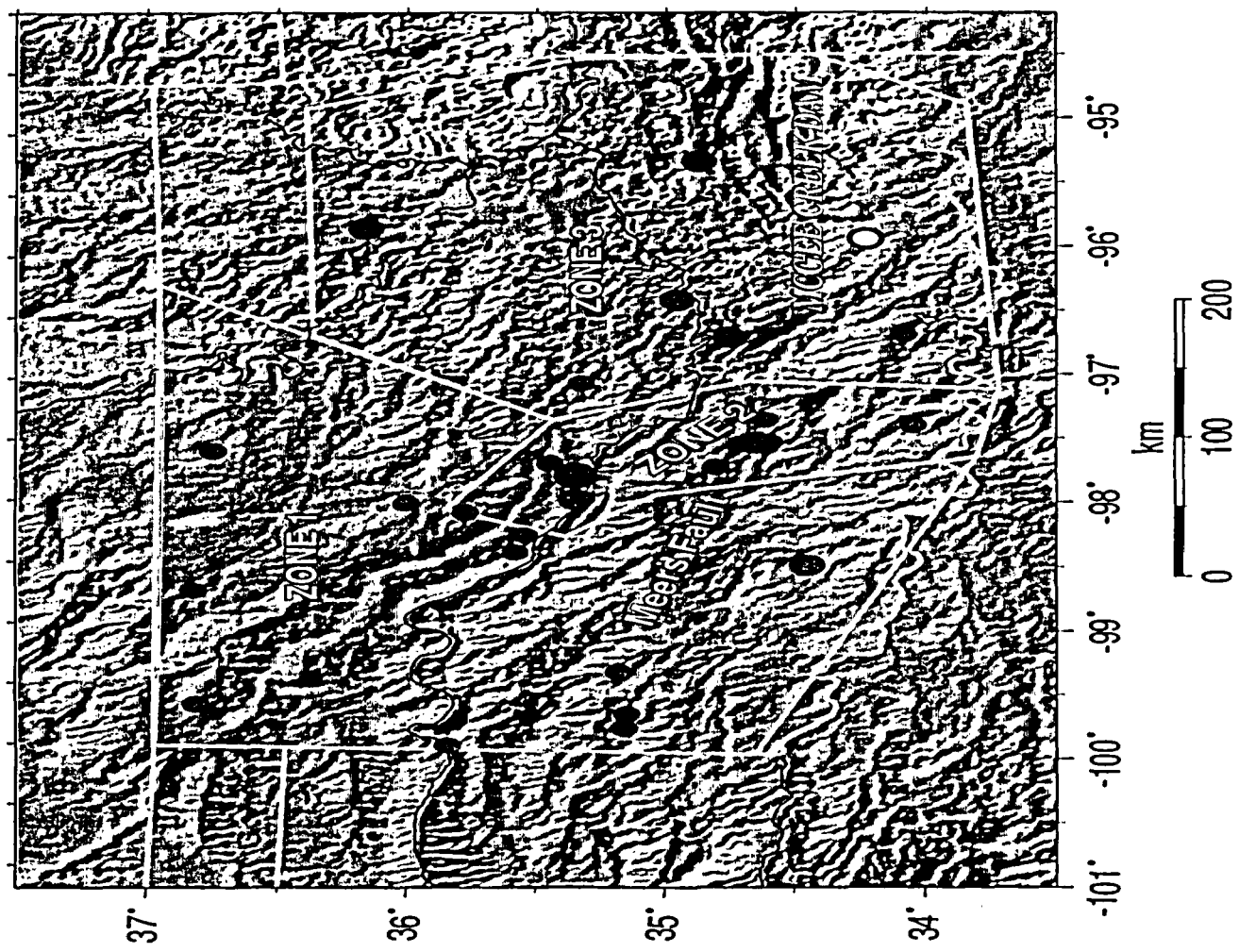

Figure 1. Location of McGee Creek Dam (white dot) and seismicity (red dots) used in hazard calculations. Earthquakes are scaled by magnitude; smallest circle is magnitude 3; largest magnitude 5. Meers fault shown as green line.

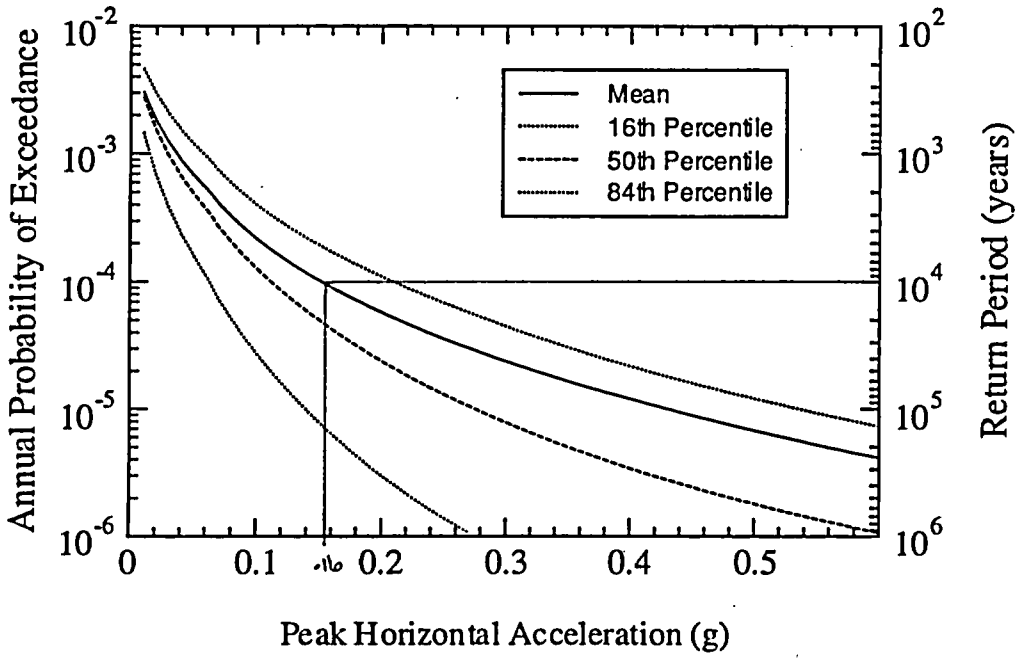

Figure 2. Mean hazard curves for PHA, McGee Creek Dam

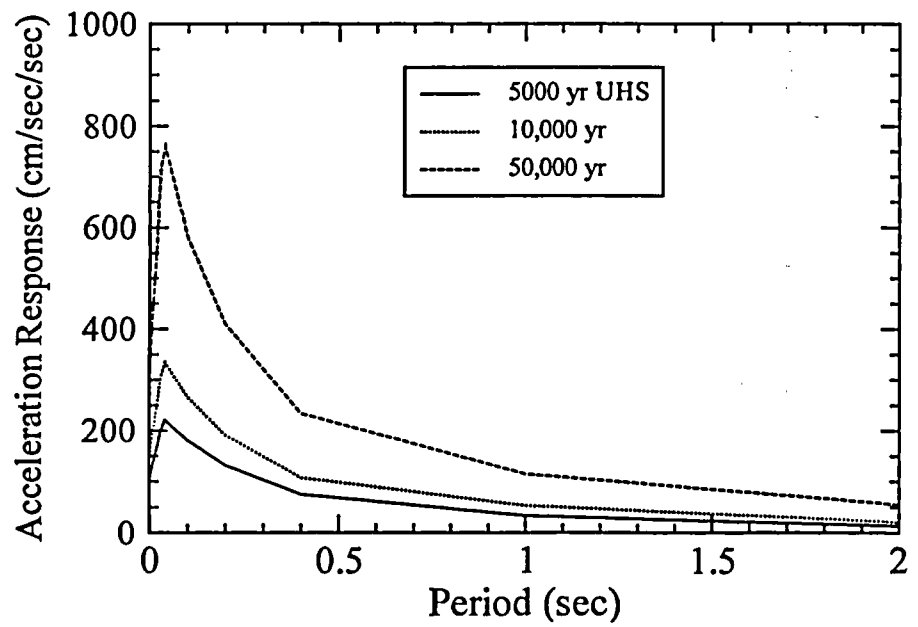

Figure 3. Mean uniform hazard response spectra, McGee Creek Dam.

Attachment 3

LaForge, Roland (2001). Selected sections from mrs Programs for Site-Specific Probabilistic Seismic Hazard Analysis for Zones of Random Seismicity, Technical Memorandum No. D 8330-2001-13, Bureau of Reclamation, June.

TECHNICAL SERVICE CENTER
Denver, Colorado

Technical Memorandum No. D8330-2001-13

mrs Programs for Site-Specific Probabilistic Seismic Hazard Analysis for Zones of Random Seismicity

Prepared by

Roland LaForge

U.S. Department of the Interior
Bureau of Reclamation

June 2001

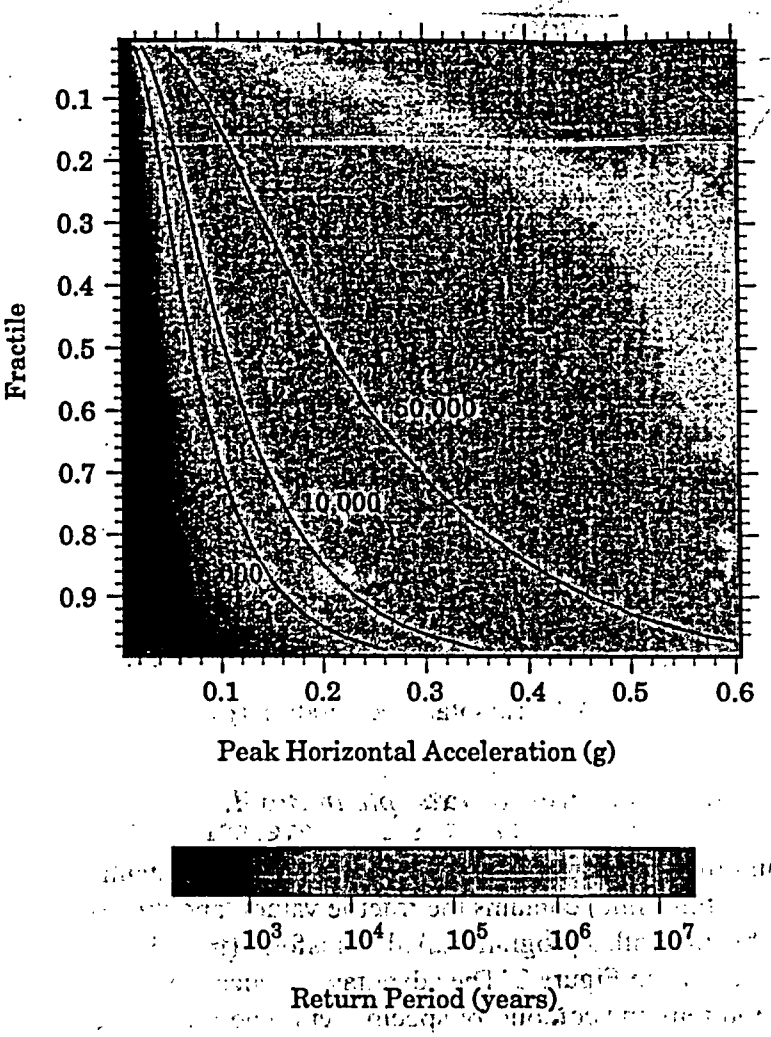

Figure 2. Cumulative distributions of ground motion exceedance, for return periods of 5,000, 10,000, and 50,000 years. Region is in the central United States.

```
  exit(0);
}
*/
```

near the bottom. The expression k == 19 refers to an acceleration level of .20 g; k == 9 would mean .10 g, etc. The `exit(0)` statement stops the program; remove it if you want it to continue.

4.0 Theory and Computation Methods

4.1 Theory

The basic formulation for probabilistic seismic hazard computation was introduced by Cornell (1968). The equation, based on the total probability theorem, is as follows:

$$P(v \geq V) = \sum_{S} \iint_{m\,r} P(v \geq V|(m,r))P(m)P(r)dmdr \qquad (1)$$

$P(v \geq V)$ is the probability that ground motion v exceeds some value V,
S is all sources,
$P(v \geq V|(m,r)$ is the probability that ground motion v exceeds value V given a magnitude and distance,
$P(m)$ is the probability of a given magnitude,
$P(r)$ is the probability of a given distance.

The left side of the equation is given in exceedances per year. The equation states that the probability of the ground motion exceeding some value is equal to the sum of the probabilities that all possible magnitudes occurring at all possible locations will exceed that value for a given source zone. The total probability for a given level is the sum of the annual frequency contributions from all sources.

It is also assumed that earthquake occurrence is a Poisson process, which means that
1) the probability of occurrence during a very small time interval Δt is given by λt where λ is the rate,
2) the probability of more than one occurrence during this interval is negligible, and
3) the probability of an occurrence during this interval does not depend on what happened prior to that time.

Use of this model thus presumes that earthquakes occur randomly in time. For large, active identifiable seismic sources it is known that larger earthquakes occur with some semblance of periodicity, and that the probability of occurence should increase as time goes on, and some occurrence models have attempted to take this into account (e.g., Cornell and Winterstein, 1988). However, for our purposes it is assumed that earthquakes occur randomly not only in time, but in horizontal space within a given source zone.

In addition to non-random behavior due to heterogeneous geologic structure and crustal stress distribution, aftershocks often occur after earthquakes of at least moderate size, and earthquakes often occur as "swarms", with no identifiable mainshock-aftershock segregation. It is therefore often necessary to "decluster" an earthquake catalog to remove such events to satisfy the Poisson criteria. A number of schemes are available for doing this; I use one based on Reasenberg (1985) (see **declust** in utils directory).

The Poisson probability distribution is given by:

$$P(x;\lambda) = \frac{e^{-\lambda}\lambda^{x}}{x!} \qquad (2)$$

where $P(x;\lambda)$ is the probability of x occurences given a rate of λ (In our scheme λ is per year). For zero occurrences, the probability is simply $e^{-\lambda}$, and the probability of 1 or more occurences $1-e^{-\lambda}$. This last expression, in our framework, is the probability that there *are* occurrences which cause exceedance of a given ground motion value, and thus is equivalent to the left hand side of

equation (1). Note that for λ of about .1 and less, $\lambda = 1\text{-}e^{-\lambda}$. Seismicity rates for the magnitude range we are interested in (≥ 5.0), annual rates are almost always below this value. Thus the terms *annual probability of exceedance* and *annual frequency of exceedance* can be considered interchangable.

4.2 The Geographical Model

P(r) in equation (1) is represented by the geographic distribution of the source zone. The programs begin by setting up a rectangular grid of points with the specified grid spacing, defined by lines 3-6 in Box 1. As each source zone is processed, points in this master set lying within the zone are identified and processed. Each point represents a square surrounding the point, whose sides are the grid spacing dimension in length, and whose area is the grid spacing squared. The seismic activity rates are scaled to this area.

The hypocentral depth distribution (for attenuation functions which use it) is approximated by a triangular distribution, with peak and maximum values as specified in line 23, Box 1. This approximation seems to be consistent with global and local observations (e.g., Strehlau, 1986). Because it is not seismologically plausible for earthquakes of magnitude ≥ 5 to have hypocentral depths at the surface, and upper limit is imposed. This depth is assumed to be the radius of a circular crack having a stress drop of 50 bars. The equation, from Kanamori and Anderson (1975) is

$$r = \left[\frac{Mo}{\Delta\sigma} \cdot \frac{7}{16}\right]^{\frac{1}{3}} \qquad (4)$$

where *Mo* is seismic moment, $\Delta\sigma$ is stress drop, and *r* is crack radius. The 50 bar value represents an average value, and can be reset in **depgenG30.c**, in pshalib. The fault dip in line 23, Box 1 represents the average dip of faults in the region, and is accounted for in calculating the minimum depths. Figure 3, from LaForge and others (1999) shows depth distributions for a range of magnitudes, used for the Sierran Foothills, California. Parameters for this example are a maximum depth of 20 km, a peak of 10, stress drop of 100 bars, and a dip of 60°.

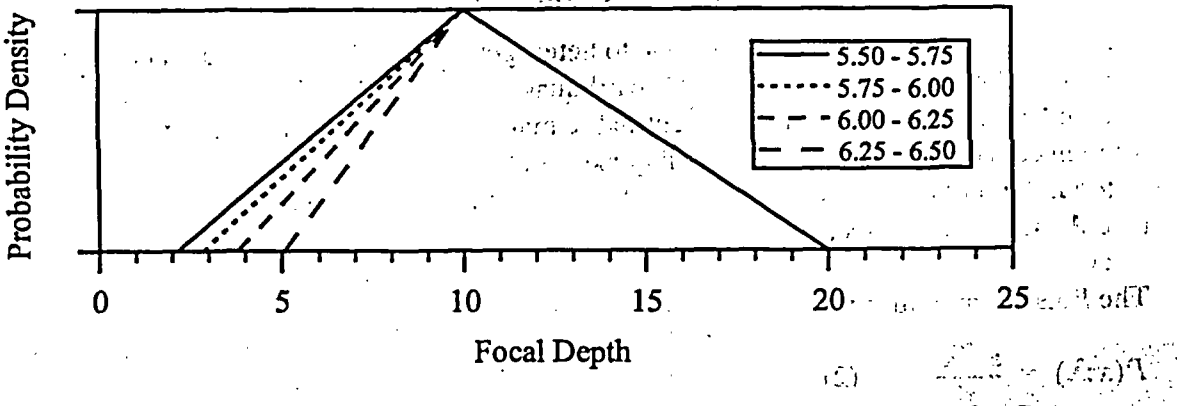

Figure 3. Hypocentral depth distributions of various magnitude ranges, for Sierran Foothills, California, from LaForge and others (1999).

if N = # of occurrences in province for y...
Na = # of occurrences per-year, per square km
Ap = Area of province
$\log(Na) = \log(N/Ap) = [a - \log Ap] - b(M)$

4.3 Seismicity Rates

P(m) in equation (1) is the magnitude rate distribution, and is where the time component enters the procedure. Magnitudes are assumed to follow the Gutenberg-Richter relation,

$$Log(N) = a - b(M) \quad (3)$$

where *N* is the number of earthquakes, and *a* and *b* are constants. When graphed, *a* is the y-intercept, and *b* is slope. In the cumulative form *N* is the number of earthquakes greater than or equal to *M*, and in the incremental form *N* is the number of earthquakes in a discrete magnitude range. In **mrs3.0** and **mrs3.1**, equation (3) is solved by the maximum likelihood technique, as described by Weichert (1980). Uncertainty distributions for discrete magnitude ranges are lognormal, and are computed as described in Bollinger and others (1989). These are incorporated directly into the probabilistic calculations. **mrs3.4** and **mrs3.5** use user-supplied *a* and *b* values for the cumulative form, and thus only provide a median estimate of seismicity rates. Because computed seismicity rates can contain a great deal of uncertainty (especially in regions where data are sparse) it is preferable to use **mrs3.0** and **mrs3.1** where possible. Recurrence parameters can be computed directly from the occurrence table, using a program called **recstat** in the utils directory.

```
West Central Montana
46139 sq km
3.00 3.50 1/1982 12/1995 12
3.50 4.00 1/1963 12/1995 13
4.00 4.50 1/1959 12/1995 9
4.50 5.00 1/1948 12/1995 3
5.00 5.50 1/1935 12/1995 3
5.50 6.00 1/1925 12/1995 0
6.00 6.50 1/1869 12/1995 1
6.50 7.00 1/1869 12/1995 1
```

Box 5 Example occurrence table

mrs3.0 and **mrs3.1** read an occurrence table, an example of which is shown in Box 5. The first line is a title, and the second line contains the area of the region considered (This region can be different that that parameterized in Box 1). The next lines contain the magnitude range, completeness period of the magnitude range, and number of events.

4.4 Attenuation Functions

$P(v \geq V|(m,r)$ is dictated by the seismicity rate and an attenuation function, which gives a lognormal distribution of ground motion amplitudes for a magnitude and distance. These are based on empirical data, but are often augmented by theoretical data in regions where observations are sparse (such as the central and eastern North America). See Seismological Research Letters, 1997, vol. 68, no. 1 for articles on recently developed attenuation functions.

To get a list of attenuation functions available for use, type **mrs3.x -l**. Although I try to code in new attenuation functions as they become available, it is possible to add new ones or your own. In the pshalib directory, the constants are defined in **attconst.h**, declared in **attrel.h**, and the computation takes place in **attrel.c**. Standard deviations of ground motion values are kept in **persigma.c**. Then add the new code and its description to **attlist.c**.

Uncertainties in the ground motion are treated by discretizing the distribution for a given magnitude and distance, and processing each discrete unit (more on the dicretization scheme in section 4.5). Because a lognormal distribution is imposed on the data, it represents an approximation. A serious consequence that arises from integrating the distribution is that the right tail of the distri-

bution (which accounts for relatively large but infrequent ground motions) has a pronounced effect on the annual frequency results for higher ground motions and longer return periods. For computational purposes the ends of the distribution must be truncated at some point (in terms of +/- $n\sigma$), and n can have a significant effect on the results (see Bender, 1984). The distribution is truncated and renormalized using a numerical method. Figure 4 shows cumulative distributions of ground motions for peak horizontal acceleration, for truncation levels of 2.0, 2.5, and 3.0 standard deviations. I have used the attenuation function of Sadigh and others (1997), and a M_W 6.0 event at a distance of 10 km. It can be seen that at fractiles of about .9 and above the difference becomes significant.

Figure 5 shows hazard curves for a site at the center of a square zone about 100 km on each side, using the attenuation function of Sadigh and others (1997), and earthquakes ranging from 5.0 to 6.5. These were made with **mrs3.4**, with a a-value of -0.9 and a b-value of -1.0. The curves show the effect of increasing the truncation point on the results; in other words allowing large ground motions to occur at the higher ground motion fractile values. At a return period of 100,000 years the discrepancy is 0.1 g. The message is that ground motion uncertainties can have a significant effect on the results, especially at longer return periods. There are few observational data to support more accurate models of ground motion amplitude behavior. In the programs the default truncation point is 2.5σ, but it can be set on the command line with **mrs3.x -z *n* ...**

4.5 Program Structure

A PSHA can be viewed as an elaborate forward earthquake ground motion simulation model. In order to have the answer reflect our current level of knowledge, input parameters are cast in the form of probability distributions as much as possible. From the probability viewpoint the procedure is Bayesian: best-guess prior distributions go in, and posterior distributions come out. The programs actually do two separate tasks: create the geographic model and generate the ground motions, and integrate the results to obtain annual frequency distributions at all ground motion levels.

The first task is shown diagrammatically in Figure 6. As with most programs, a loop structure is employed. Note that for **mrs3.4** and **mrs3.5** Rate Distribution is a single value for each magnitude interval, and for **mrs3.1** and **mrs3.5** Spectral Period is a single value. The number of discretization points for Rate Distribution is set in **mrs3.0.h** and **mrs3.4.h** as RATEPCT. A value of 20 appears to give stable results (i.e., a greater value does not visibly change the results). A number of points for Ground Motion Distribution (GMPCT) and Depth Distribution (NDEPTHS) are also necessary; I have found values of 50 and 5, respectively, to give stable results. If we take as a typical example a square source region 100 km on a side with the site at the center, with a 5 km grid spacing, this gives 400 grid points. With, for example, 6 magnitude values, this means that for a single response period Attenuation Function is accessed 20 x 50 x 5 x 400 x 6 = 12,000 times. In order to decrease computation time the attenuation function is set up as a look-up table.

The second part of the task is sorting the annual frequencies into the appropriate ground motion exceedance bins, and integrating to obtain cumulative probability density functions at each ground motion level. In the example above, I refer to the 12,000 "answers" as "models", since each represents a possible behavior of the overall seismic source model. Looking at Figure 6,

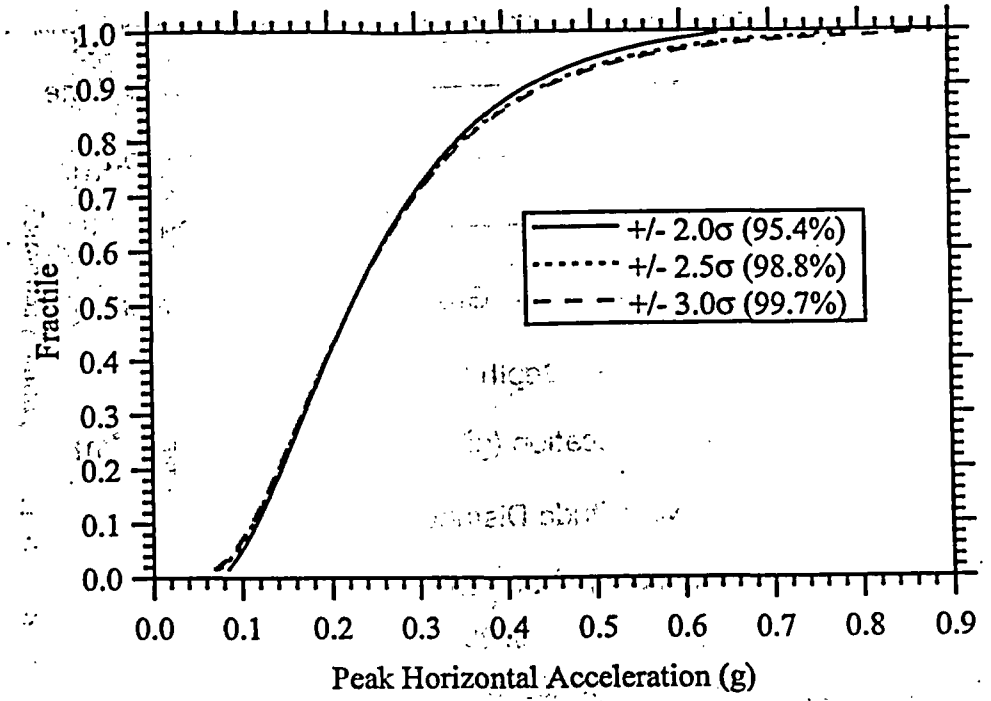

Figure 4. Cumulative ground motion distributions for various truncation/renormalization levels, for a M_W 6.0 event at a distance of 10 km, using Sadigh and others (1997) attenuation. Percentage of untruncated distribution used is indicated.

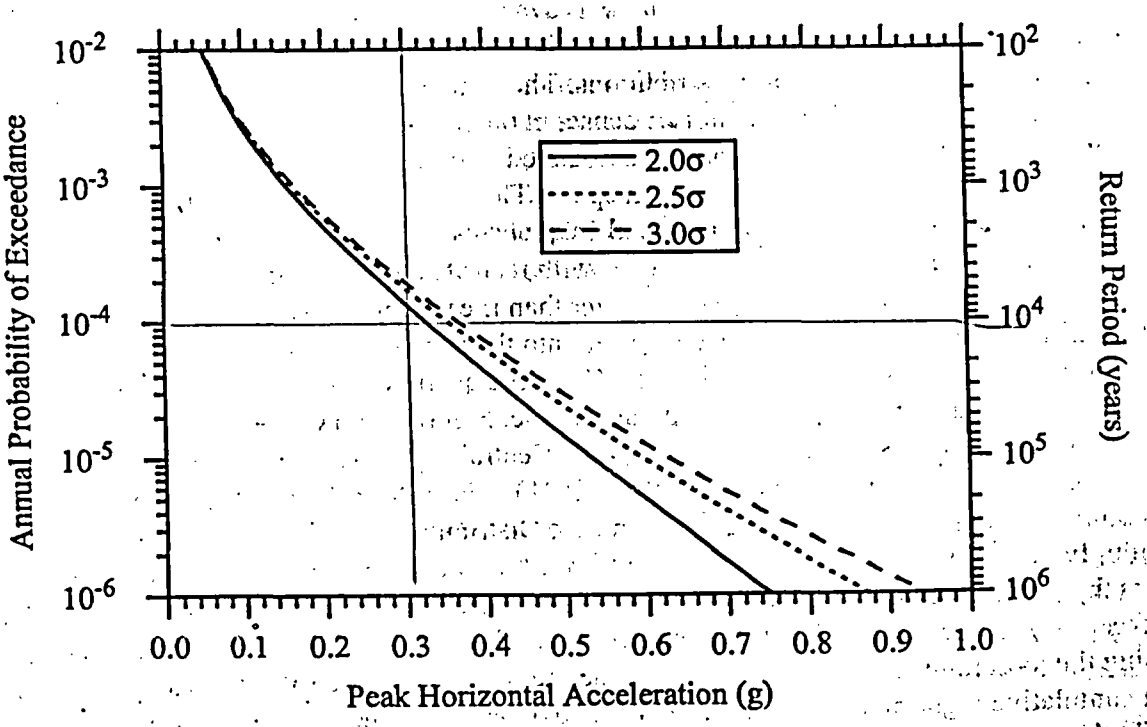

Figure 5. Hazard curves for a typical random source zone, showing the effect of using different truncation points in the ground motion distributions (see text).

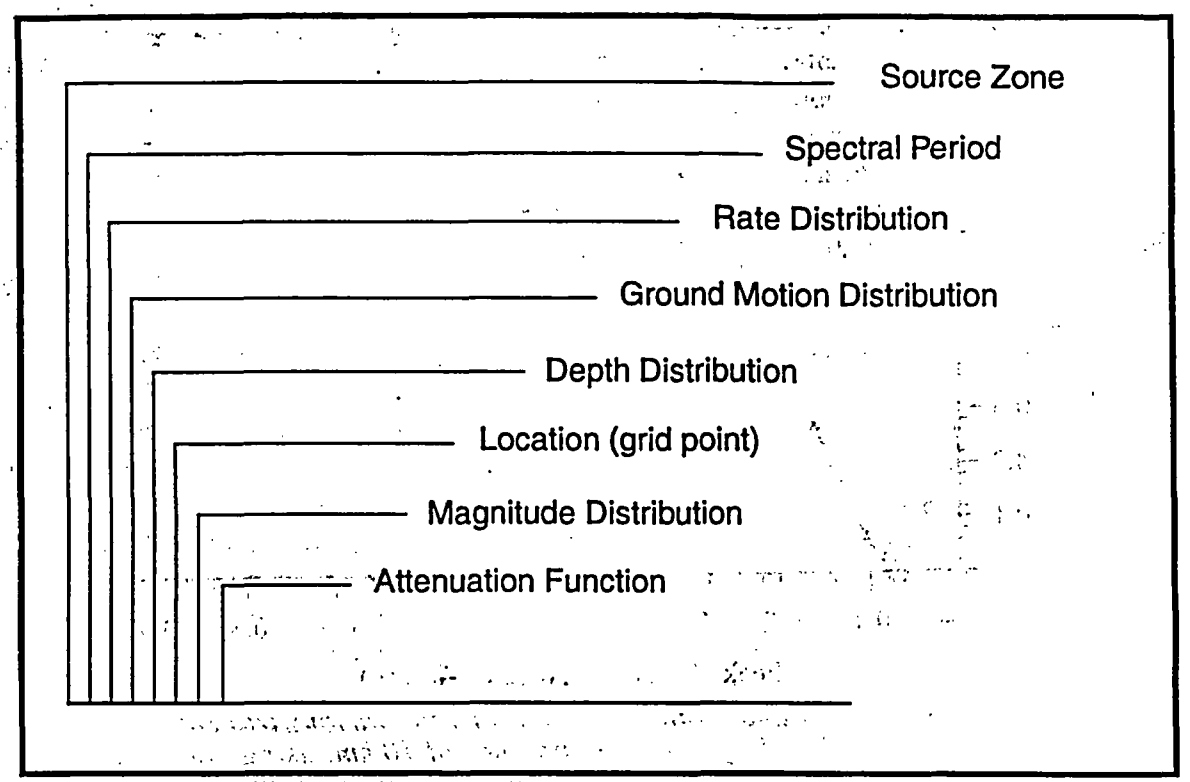

Figure 6. Program loop structure.

below Spectral Period all inputs are distributions. The Rate, Ground Motion, and Depth distributions are discretized in an *equal probability* sense, in other words, the distributions are divided such that each unit has an equal probability associated with it. The gridpoints are also equal probability, since we are assuming randomness in space. The probabilities for the Magnitude Distribution are the annual occurrence rates (or annual frequencies), derived from the recurrence calculations. Thus each "model", which carries with it an annual frequency, has an equal probability of occurring. This makes the integration faster than if each model has a different weight. Once the annual frequencies for each model are sorted into the appropriate exceedance bins, they are sorted from lowest to highest in each bin. The C routine qsort is used for this purpose, and this takes the largest fraction of the total computation time. Figure 7 shows the annual frequency distribution for exceedances of 0.20 g, from the West Central Montana source zone of Box 1. The total number of models shown here is 20 (RATEPCT) x 50 (GMPCT) x 5 (NDEPTHS) = 5,000. Each point includes all the Location and Magnitude Distribution points; otherwise we would have to multiply 5,000 by 704 (number of gridpoints) x 6 (number of magnitude intervals) = 21,120. This is the actual number of models. (The deaggregation analysis requires this kind of detailed bookkeeping). Since these additional distributions are the same for each point plotted, the effect of using the total number would be to simply change the x-axis scale values. Note that the curve has a cumulative lognormal appearance; this is understandable since the two non-uniform input distributions are lognormal.

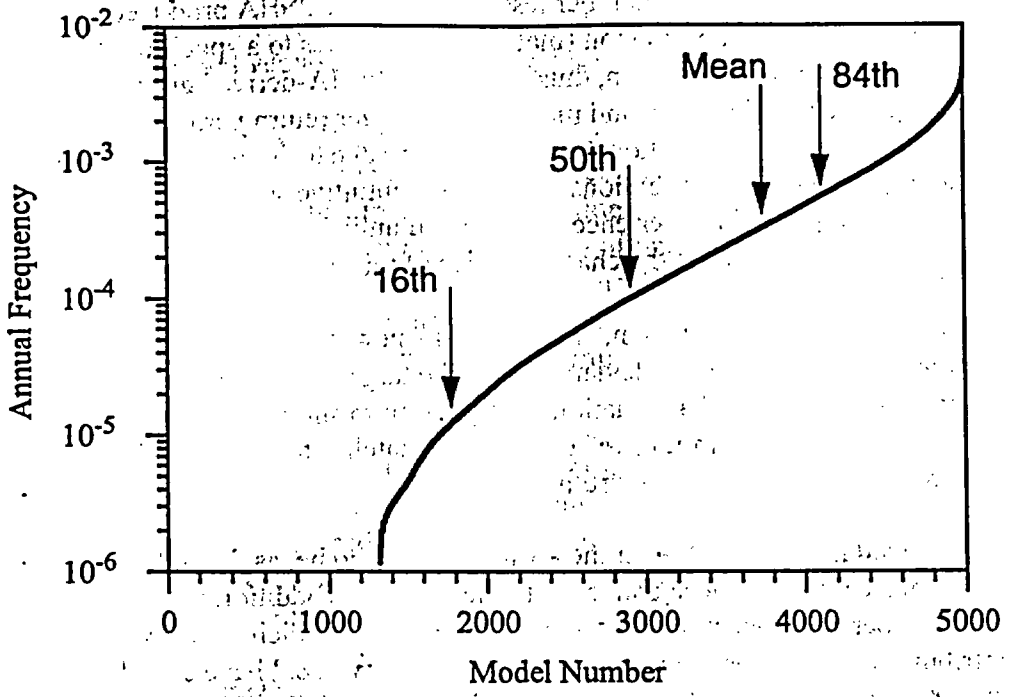

Figure 7. Sorted models for exceedances of 0.20 g, West Central Montana source of Box 1. Fractile values and mean are noted.

Out of the 5,000 models in Figure 7, 1,320 have an annual frequency of zero. This is because we are incorporating a lognormal ground motion distribution, and for this case, even for nearby events there is a probability that the ground motion will not reach 0.20 g. For values larger than 0.20 g there will be fewer non-zero models; for smaller values there will be more. The annual frequencies must therefore be multiplied by the probability that the source model generates exceedances of 0.20 g, or simply the number of non-zero models divided by the total number of models. This is why the median annual frequency value in figure 7 does not simply correspond to the midpoint of the non-zero models, but is something less.

5.0 Deaggregation

5.1 Introduction

Deaggregation is a process by which the contributions of magnitude, distance, and other parameters to a particular ground motion exceedance level are collected and turned into probability density functions (pdfs) or probability mass functions (pmfs). From these, average values are often extracted and used in the selection of accelerogram records for use in dynamic analysis of engineered structures. These are often called "design earthquakes". The most common of these is average magnitude ($\overline{M}$, or "M-bar") and average distance ($\overline{D}$, or "D-bar").

Because deaggregated $\overline{M}$ and $\overline{D}$ do not take into account the fact that the ground motion distribution that went into the PSHA was actually not a point value but a distribution, taking the $\overline{M}$ and $\overline{D}$